Sedimentary talc in Neoproterozoic carbonate successions

Sedimentary talc in Neoproterozoic carbonate successions

Nicholas J. Tosca[1*], Francis A. Macdonald[2], Justin V. Strauss[2], David T. Johnston[2], Andrew H. Knoll[2,3]

[1] Department of Earth Sciences, University of Cambridge, Cambridge, CB2 3EQ, UK
[2] Department of Earth and Planetary Sciences, Harvard University, Cambridge, MA 02138, USA
[3] Department of Organismic & Evolutionary Biology, Harvard University, Cambridge, MA 02138, USA
*****Corresponding author: njt41@cam.ac.uk*; T: +44 (0)1223 333442; F: +44 (0)1223 333450

Abstract

Mineralogical, petrographic and sedimentological observations document early diagenetic talc in carbonate-dominated successions deposited on two early Neoproterozoic (~800-700 million years old) platform margins. In the Akademikerbreen Group, Svalbard, talc occurs as nodules that pre-date microspar cements that fill molar tooth structures and primary porosity in stromatolitic carbonates. In the upper Fifteenmile Group of the Ogilvie Mountains, NW Canada, the talc is present as nodules, coated grains, rip-up clasts and massive beds that are several meters thick. To gain insight into the chemistry required to form early diagenetic talc, we conducted precipitation experiments at 25°C with low-SO_4 synthetic seawater solutions at varying pH, Mg^{2+} and SiO_2(aq). Our experiments reveal a sharp and reproducible pH boundary (at ~8.7) only above which does poorly crystalline Mg-silicate precipitate; increasing Mg^{2+} and/or SiO_2(aq) alone is insufficient to produce the material. The strong pH control can be explained by Mg-silica complexing activated by the deprotonation of silicic acid above ~8.6-8.7. FT-IR, TEM and XRD of the synthetic precipitates reveal a talc-like 2:1 trioctahedral structure with short-range stacking order. Hydrothermal experiments simulating burial diagenesis show that dehydration of the precipitate drives a transition to kerolite (hydrated talc) and eventually to talc. This formation pathway imparts extensive layer stacking disorder to the synthetic talc end-product that is identical to Neoproterozoic occurrences. Early diagenetic talc in Neoproterozoic

carbonate platform successions appears to reflect a unique combination of low Al concentrations (and, by inference, low siliciclastic input), near modern marine salinity and Mg^{2+}, elevated $SiO_2(aq)$, and pH > ~8.7. Because the talc occurs in close association with microbially influenced sediments, we suggest that soluble species requirements were most easily met through microbial influences on pore water chemistry, specifically pH and alkalinity increases driven by anaerobic Fe respiration.

Keywords: Proterozoic; geobiology; mineralogy; geochemistry; carbonate; silica

1. Introduction

Talc, $Mg_3Si_4O_{10}(OH)_2$, is typically interpreted as a high-temperature mineral that forms from hydrothermal alteration or metamorphism of Mg-rich and ultrabasic rocks (Evans and Guggenheim, 1988; Marumo and Hattori, 1999). Lower temperature reactions can also produce talc-bearing assemblages, for example through the weathering of serpentinite deposits (Velde and Meunier, 2008); however, this class of reactions is far less common than its high temperature counterpart. As such, outside of the scattered reports of talc in evaporite or carbonate rich deposits (Bodine, 1983; Braitsch, 1971; Calvo et al., 1999; Friedman, 1965; Millot and Palausi, 1959; Noack et al., 1989), talc is rarely reported as a sedimentary mineral. Here we document the unusual occurrence of early diagenetic talc associated with Neoproterozoic (~800-700 Ma) carbonates deposited on two separate platform margins: the Akademikerbreen Group in Svalbard and the Fifteenmile Group in the Ogilvie Mountains of northwestern Canada. The formation of sedimentary talc and its mineralogical precursors requires a specific set of chemical conditions;

its presence places tight quantitative constraints on Neoproterozoic ocean chemistry and provides additional insight into the biogeochemistry of marine sediments at that time.

At low temperatures (i.e., less than ~30^{o}C), the Mg-silicate system is controlled mainly by kinetic phenomena (Evans and Guggenheim, 1988; Jones, 1986; Wollast et al., 1968), and so constraints on early diagenetic chemistry are difficult to derive based on thermodynamics alone. To address this problem, we designed a series of experiments to evaluate the effects of changing pH, Mg^{2+} and SiO_2(aq) on the formation of Mg-silicates from low-SO_4 (~2.8 mmol/kg), Neoproterozoic-like seawater solutions. When these experiments and companion modeling results are coupled with stratigraphically constrained geochemical data, we are able to posit that the early diagenetic talc in Neoproterozoic carbonate successions reflects a unique combination of low siliciclastic input, near marine salinity and Mg^{2+}, elevated SiO_2(aq), and pH greater than ~8.6-8.7. In what follows, we discuss: (1) the sedimentology, geochemistry and mineralogy of the Akademikerbreen and Fifteenmile talc occurrences, (2) experimental constraints on Mg-silicate formation from modified Neoproterozoic-like seawater solutions, and (3) reports of similar mineral assemblages from other Neoproterozoic successions. Finally, we consider both the specific constraints these data place on the chemistry of waters bathing Neoproterozoic carbonate platforms and why this interval in Earth history may have favored sedimentary talc formation.

2. Geologic Setting

Sedimentary talc occurs in Neoproterozoic strata that crop out discontinuously over a distance of more than 140 km in the Coal Creek and Hart River inliers of the Ogilvie Mountains, Yukon (for exact locations see Macdonald and Roots, 2009). The talc is stratigraphically

confined to the lower Callison Lake Dolostone (unit PF2 of the Fifteenmile Group), which consists predominantly of dolomite with interbedded shale (Fig. 1 & 2) (Macdonald and Roots, 2009; Macdonald et al., 2010). A tuff within the lowermost map unit of the Fifteenmile Group provides a maximum age constraint on the talc of 811.51 ± 0.25 Ma; a minimum constraint comes from a 717.43 ± 0.14 Ma quartz-phyric rhyolite flow in the overlying Mount Harper volcanic complex (Macdonald et al., 2010).

On a ridge ~10 km to the northwest of Mt. Harper, the lower Callison Lake Dolostone is well exposed and measures 77 m thick (Macdonald and Roots, 2009). Here, these strata rest unconformably on a brecciated surface of PF1 platformal carbonate and consist of a basal 2 m of channelized, sub-rounded quartz gravel conglomerate. These beds are overlain by 17 m of green and red shale and siltstone with dolomite lenses containing microbialite textures. The microbialite is draped with a ~10 cm thick bed of hematite iron formation. Above the varicolored shale and siltstone are an additional 60 m of black shale with laterally discontinuous dolomitic bioherms and abundant microbialite. However, the black shale has a peculiar waxy luster, reminiscent of phosphorite, and XRD analyses indicate that this shale consists almost exclusively of talc. The black talc-bearing shale also contains lenses of redeposited talc rip-up clasts suspended in fine-grained dolomite matrix and abundant black chert nodules. These strata are succeeded gradationally by over 300 m of silicified dolostone (Unit PF3), dominated by stromatolites, microbialaminite, and edgewise conglomerate with cm-sized coated grains, occasional exposure surfaces, and patchy silicification. These facies all suggest deposition in a shallow-water, episodically exposed, marginal marine environment.

The talc is stratigraphically confined and laterally persistent along the outcrop belt for over 30 km to the east to Mt. Gibben, and occurs again an additional ~110 km to the east in the

Hart River inlier (Abbott, 1997). This lateral extent suggests that talc deposition was at least a basin-wide phenomenon. The Fifteenmile Group has been correlated with the Little Dal Group in the Mackenzie Mountains (Macdonald et al., 2010), which has been interpreted as a marginal marine carbonate bank deposited on a rifted passive margin (Turner and Long, 2008). However, the significant unconformity recently identified at the base of the Callison Lake Dolostone suggests that it may have formed in an additional distinct basin-forming episode (Macdonald and Roots, 2009), perhaps coeval with the Coates Lake Group, which lies stratigraphically above the Little Dal Group. The Coates Lake Group was deposited in narrow, restricted grabens (Jefferson and Parrish, 1989). Although neither evaporitic minerals or pseudomorphs have been identified in the Fifteenmile Group, evaporites are present in both the Little Dal and Coates Lake groups (Jefferson and Parrish, 1989), and we cannot rule out restriction on the platform.

In Svalbard, mm to cm scale talc nodules occur within shallow marine carbonates of the Hunnberg Formation, Nordaustlandet, and its lateral equivalents in Spitsbergen, the upper Grusdievbreen and Svanbergfjellet formations (Fig. 2 & 3; Knoll and Swett, 1990). As in Canada, the talc deposits occur in settings ranging from coastal to subtidal environments below storm wave base and can be traced along strike for several hundred kilometers, suggesting a basin-scale phenomenon. Also as observed in Canada, cm-scale hematite layers drape microbial dolomites in the talc-bearing interval. In the Svanbergfjellet Formation, talc forms cm-scale nodules within relatively deep carbonaceous shales and carbonates. More extensive and striking, however, are rounded nodules that formed within molar tooth structures and primary voids in microbialites, in both cases before penecontemporaneous void-filling microspar cements were deposited (Fig. 3; Knoll, 1984, who mistakenly identified the talc nodules as phosphorite).

No radiometric dates closely constrain the age of talc-bearing Svalbard carbonates, but C and Sr isotopic chemostratigraphy and biostratigraphy suggest an age broadly comparable to that of the Ogilvie succession (Halverson et al., 2007; Knoll et al., 1986; Macdonald et al., 2010).

3. Analytical and experimental methods

Our sample suite was selected from the lower Callison Lake Dolostone of the Fifteenmile Group and from throughout the Akademikerbreen Group (Fig. 2; Table 1). The Fifteenmile Group samples, all from outcrop, include dolostone hosting nodular talc, bedded talc deposits, and a small horizon of iron formation. With the exception of some visible surface staining, late stage alteration/oxidation of the samples generally appears minor. Samples from the Akademikerbreen Group are predominantly from the Svanbergfjellet Formation and correlative horizons in the Hunnberg Formation, where nodular talc was identified in the field, but they also include carbonates and shales from units above and below this interval. All Svalbard samples were collected from outcrop and were chosen to capture the range of carbonate lithofacies reported in Knoll and Swett (1990). Again, late stage alteration/oxidation is minor in Svalbard samples, as documented by geochemical screens (e.g., Sr concentration, Mn/Sr, Sr/Ca and $\delta^{18}O$; Derry et al., 1989).

Mineralogical analyses included X-ray diffraction (XRD) of <2μm (and in some cases, <0.2μm) oriented aggregates from decarbonated samples, and bulk XRD of unfractionated samples. Petrographic analysis and electron microprobe analysis of selected samples were performed using polished, carbon-coated thin sections. Further details of sample preparation and analysis are given in the Supplementary file.

142 Precipitation experiments were performed by addition of SiO_2(aq) to 1 kg batches of
143 synthetic low-SO_4 seawater at various Mg^{2+}(aq) concentrations and pH. Experiments were run in
144 water baths at 25 ±0.1°C for a minimum of 4-5 weeks to a maximum of 7 months, depending on
145 conditions. Filtered aqueous samples were collected periodically and analyzed by ICP-AES, and
146 residual solid precipitates were collected at experiment termination, washed and analyzed by
147 XRD, FT-IR and TEM. Selected solid precipitates were extracted and reacted with deionized
148 water at 180°C and 400°C to evaluate mineralogical changes in response to heating/dehydration.
149 Further details of the experimental and analytical procedures are given in the Supplementary file.
150
151 **4. Mineralogy and petrography of Neoproterozoic talc**
152 *4.1 Fifteenmile Group*
153 Nodular talc samples from the Callison Lake Dolostone have three components in
154 varying proportions: dolomite, chert, and talc. Detrital siliciclastic input is apparent only in the
155 lower 40 m of varicolored shale and siltstone with interbedded microbial dolomite (Fig. 2). The
156 thin horizon (~10 cm) of iron formation that drapes the microbialite is mineralogically simple,
157 consisting of euhedral hematite grains dispersed in a dolomite matrix, with minor silicification
158 and rare detrital quartz grains. <2μm size fractions reveal a single 7Å kaolin-serpentine group
159 phase with trioctahedral occupancy, consistent with greenalite. The dolomite is present both as
160 primary microbial laminations, coated grains, and as interstitial microspar cement. Talc both
161 drapes and fills laminae within the microbialites and, along with the black chert, forms early
162 diagenetic nodules. Bedded chert is also common. In silicified dolostones of the Callison Lake
163 Dolostone that host nodular talc, carbonate mineralogy consists exclusively of dolomite, with no
164 calcite indicated from powder XRD. Aside from talc, the clay mineralogy of decarbonated

samples indicates lesser amounts of either discrete highly crystalline illite and/or mixed layer illite/smectite. The composition of the mixed layer phases is highly consistent from sample to sample, and analyses after ethylene glycol treatment are consistent with R0 (disordered) illite(0.7)/smectite.

The bedded talc horizons consist predominantly of black, talc-rich shale. Thin lenses of sub-angular to sub-rounded rip-up clasts of talc supported by very fine-grained dolomite matrix are interbedded with the talc horizons. The interstitial dolomite cements between the reworked talc clasts suggest that at least some of the talc formation predates the formation of these particular cements. The mineralogy of bedded talc samples is also simple; talc overwhelms bulk analyses and clay fractions in abundance. However, two samples of bedded talc revealed subordinate amounts of discrete highly crystalline illite and mixed layer R0 illite(0.7)/smectite (Table 1). In contrast to bulk samples, oriented <2μm size fractions of bedded talc indicate that no mixed layering is apparent. In other words, the talc is present as a discrete mineral phase. No other Mg-silicates were identified in any bulk or <2μm fractions from Fifteenmile Group samples (Fig. 4). Randomly oriented specimens of the <2μm clay fraction further indicate that the talc exhibits a high degree of stacking disorder; it is essentially turbostratic. A number of *hkl* peaks are significantly modulated, particularly in the 20-25 degree and 30-45 degree range. This type and extent of disordering is present in all of the Fifteenmile talc occurrences.

The carbonate overlying the talc horizons consists of silicified dolomite with microbial lamination, coated grains, and abundant stromatolites. Void-filling cements consist predominantly of dolomite and silica. Decarbonated samples from these strata also yielded talc with lesser amounts of discrete illite and mixed layered illite/smectite. The talc in these samples

187 is distributed throughout the carbonate matrix and not as nodules or other conspicuous
188 sedimentary features otherwise resolvable by petrographic analysis.
189
190 *4.2 Akademikerbreen Group*
191 Akademikerbreen talc occurs as mm- to cm-scale nodules and disseminated particles in
192 the <2μm fraction of the carbonate matrix. Talc nodules fill molar tooth structures, primary void
193 space in microbialites and intergranular space, predating precipitation of penecontemporaneous
194 microspar cement. In general, nodules are petrologically homogeneous; there are no discernable
195 nuclei nor is chemical zoning evident (Fig. 3).
196 Powder XRD of isolated and cleaned nodules hand picked from Akademikerbreen
197 carbonates shows the same type and extent of layer stacking disorder as in the Fifteenmile talc
198 samples (Fig. 5). That is, the Akademikerbreen talc is also highly turbostratic. XRD patterns
199 again display modulated and/or extinguished *hkl* reflections in the 20-25 and 30-45 degree 2Θ
200 ranges. Aside from talc, the carbonate mineralogy frequently includes ankerite in addition to
201 dolomite and lesser amounts of calcite.
202 The clay mineralogy of decarbonated Akademikerbreen samples shows more variation
203 among the Mg-silicates. Analyses of decarbonated residues reveal talc in the carbonate matrix in
204 some samples where nodules are not apparent. The talc again shows no evidence of mixed
205 layering or occurrences with other low temperature Mg-silicates such as sepiolite or palygorskite.
206 However, saponite (a Mg-rich trioctahedral smectite) and its burial diagenetic equivalents, mixed
207 layered chlorite/smectite and corrensite, have all been identified (Fig. 4; Table 1; Supplementary
208 file).

In addition to Mg-silicates, Akademikerbreen clay fractions contain varying amounts of discrete highly crystalline illite, illite/smectite (most of which corresponds to R1 illite(0.7)/smectite), kaolinite, and, in one sample only, chlorite. In general, the results summarized in Table 1 show that samples containing talc and other associated Mg-silicates consistently lack illite, I/S, and kaolinite. The reverse is also true: aluminous clay mineral assemblages are rarely accompanied by talc.

The Svanbergfjellet, Draken and Backlundtoppen Formations also contain discrete siliciclastic horizons that represent detrital pulses into the carbonate platform (Butterfield et al., 1994; Knoll and Swett, 1990). The clay mineralogy of these horizons is dominated by illite and kaolinite in the <2μm fraction; the <0.2μm fraction is composed almost entirely of discrete illite, with significant defect broadening.

4.3 Fifteenmile and Akademikerbreen Group Mg-silicate occurrences: Summary

Sedimentology and petrology indicate that talc formed during early diagenesis, perhaps penecontemporaneously, in both the Akademikerbreen and the Fifteenmile Groups. In both environments the clay mineralogy also indicates that talc generally occurs in environments that received low background siliciclastic flux, and where alumino-silicates are present, talc has not been identified.

Saponite, chlorite/smectite and corrensite in Akademikerbreen carbonates, all indicate that saponite formed during early diagenesis and was transformed to chlorite-rich mineral species upon burial and late-stage alteration. Because there is little evidence for mafic input to the Akademikerbreen platform, saponite formation suggests that the initial deposition of smectite (originally as a dioctahedral smectite such as montmorillonite), or some other detrital precursor,

initiated a recrystallization/transformation to trioctahedral saponite, likely in response to favorable aqueous chemistry associated with the platformal carbonates (discussed below).

Samples from the Fifteenmile Group, on the other hand, yield very little decarbonated residue and show little variation in background siliciclastic component; they are dominated by highly crystalline illite (muscovite) and illite/smectite. Together this implies very low background detrital fluxes and negligible input of terrigenous clay beyond detrital muscovite.

The sedimentology, petrography and mineralogy of these deposits are indicative of unusual aqueous chemistry associated with platformal carbonates that facilitated the early diagenetic precipitation of Mg-silicates, whether talc or a precursor phase, from solution. What drove these reactions during Akademikerbreen and Fifteenmile Group deposition?

5. Constraints from Mg-silicate precipitation experiments

To better understand what chemical environment is required to initiate the precipitation of Mg-silicates, we performed a systematic series of experiments interrogating the role of SiO_2(aq) and pH on talc formation. We incubated one liter batches of standard, "modern" synthetic seawater at various SiO_2(aq) concentrations and pH, monitoring the bottles for both precipitation of solid phases and changes in aqueous chemistry. In certain experiments, a visible precipitate formed within the first 48 hours. The precipitate often clouded the solution before flocculating and, eventually, settled to the bottom of the reaction vessel. In other experiments, no precipitate was formed over > 7 months.

When the experimental conditions favored precipitation, XRD analyses on randomly oriented powders showed broad and poorly resolvable *hkl* bands and no 001 reflections (Fig. 5). All XRD analyses showed weak bands at d = 1.55 to 1.52Å, indicating the presence of

255 trioctahedral layers, and all *hkl* bands were reproducible from experiment to experiment,
256 displaying little variation in their relative intensity and *d*-spacing. In only one case, the
257 experiment conducted at the highest pH, a precipitate gave broad low-angle reflections
258 corresponding to *d*-spacings of 28.7, 13.9 and 10.4 Å. With the exception of the highest pH
259 experiment, the structure of the precipitate is both insoluble and reproducible from experiment to
260 experiment. Perhaps most striking, however, is the observation that the precipitate only formed at
261 a pH of 8.66 and above, implicating pH as a major control on Mg-silicate precipitation.

262 Although XRD data show poorly crystalline products, FT-IR spectra indicate that the
263 experimental precipitates are almost identical to talc. The close correspondence between Mg-O
264 vibrations from the precipitates and lattice vibrations from talc (including the diagnostic 535 cm^{-1}
265 (Mg-O)-OH feature (Farmer, 1974; Zhang et al., 2006)) reflect a similar bonding environment
266 for Mg (Fig. 6). Absorptions at ~1020 cm^{-1} show the same bonding arrangement for SiO_4
267 tetrahedra: a 2:1 layered configuration of tetrahedral silicate layers and octahedral MgO_6 layers
268 (Fig. 6). A trioctahedral occupancy (consistent with XRD peaks at 1.55-1.52 Å), manifested by
269 the OH-stretching vibration at ~3676 cm^{-1}, is also evident for both the precipitates and for talc
270 standards. However, the lack of an observable basal 001 reflection in oriented XRD patterns
271 suggests that there is little to no stacking order between TOT sheets, perhaps due to variable
272 interlayer/surface hydration (consistent with absorptions at ~1630 and ~3400 cm^{-1} indicating
273 appreciable bound molecular H_2O). Taken together, XRD, FT-IR and TEM data (shown in the
274 Supplemental File) indicate the experimental precipitates are simply a hydrated, disordered form
275 of talc; they are composed of 2-dimensional talc TOT sheets not neatly stacked as in true talc,
276 but organized similar to a pile of bricks loosely cemented with water of hydration.

To ascertain the effects of mild heating on poorly crystalline Mg-silicate precipitated from modified seawater solutions, we also performed experiments involving the hydrothermal treatment of poorly crystalline Mg-silicate (the products of precipitation experiments) in the presence of deionized water. After 4 weeks of reaction at 180°C, the poorly crystalline Mg-silicate transformed to kerolite ($Mg_3Si_4O_{10}(OH)_2 \cdot nH_2O$), a distinct mineral phase and hydrated structural analog of talc (Fig. 5). The final product exhibited an apparent *d*(001) of 9.9 Å and *hkl* peaks that correspond to the kerolite structure discussed in Brindley et al. (1977). Combined XRD, FT-IR and TEM data indicate that simple dehydration -- in this case, in response to temperature increase – drives the transformation from poorly crystalline Mg-silicate to the mineral kerolite. Further heating at elevated temperature or over long timescales in turn causes additional dehydration and experiments conducted at 400°C and 1kbar show that this dehydration drives the transition from kerolite to talc (and minor cristobalite) (Fig. 5). The talc produced from this process exhibits significant turbostratic ordering and powder diffraction data show similar peak modulation to Neoproterozoic talc samples discussed above.

6. Discussion

6.1 Mg-silicate system at low temperature

Present-day seawater is supersaturated with respect to crystalline talc, yet modern and even ancient environments lack authigenic talc (Fig. 7). Like in the case of carbonate precipitation, there must exist a kinetic barrier to talc precipitation; a barrier that we can address through experimental interrogation. Our data and ensuing discussion allow talc precipitation to be reconstructed in an environmentally tuned, step-wise fashion.

299 Previous experimental work has targeted talc precipitation from modern-like seawater,
300 and presents contrasting results to those described herein. Wollast et al. (1968) spiked filtered
301 modern seawater with sodium metasilicate (Na_2SiO_3:$9H_2O$) at 25°C and precipitated a Mg-
302 silicate phase at pH > 8.3. The Mg-silicate was described as "poorly crystalline sepiolite" on the
303 basis of FT-IR and XRD -- a phase not identified in any of our experiments. In addition, the
304 apparent solubility calculated from their experiments is lower than the experiments described
305 here (Fig. 7), implying a lower degree of supersaturation needed for precipitation. Upon closer
306 inspection, however, the Mg-silicate precipitated by Wollast et al. (1968) is not inconsistent with
307 our results. In fact, their FT-IR and XRD analyses also lack the most diagnostic features of
308 sepiolite, including the 12 Å and 7.5 Å diffraction peaks and a Si-O feature in FT-IR attributed to
309 Q_3 bonding of silica tetrahedra in chain silicates (Russell and Fraser, 1994). However, their
310 material also appears to exhibit FT-IR features that ours does not.
311 Aside from the identity of the initial precipitate, there also remains a clear discrepancy in
312 the literature in the aqueous conditions needed to initiate precipitation. To address this, we
313 duplicated some of the experiments conducted by Wollast et al. (1968) using a synthetic
314 "modern" seawater solution at elevated SiO_2(aq). The only difference is the nature of the silica
315 source: TEOS solutions in experiments described here versus sodium metasilicate solutions in
316 Wollast et al. (1968). The results show that Mg-silicate formation does not occur until higher
317 levels of supersaturation than those reported by Wollast et al. (1968) and that the initial
318 precipitate is a known kerolite precursor. We argue that the difference in silica source may well
319 be critical. We have taken precautions to ensure that SiO_2(aq) added to seawater solutions was
320 equilibrated in the monomeric form prior to the addition of $MgCl_2$ (Dietzel, 2000; Iler, 1979). In
321 contrast, sodium metasilicate solutions are known to polymerize rapidly and form colloidal

material upon dilution (Iler, 1979), perhaps in response to decreasing silica levels and/or rapid changes in pH associated with their preparation. Thus, it is possible that the addition of metasilicate solutions to seawater solutions co-precipitated silica with Mg^{2+} in a way that may not be truly representative of natural surface environments. This is a complication avoided in our experiments through the use of TEOS as a $SiO_2(aq)$ source.

6.2 Mg-silicate formation: pH as a master variable

To assess what special combination of Mg^{2+}, $SiO_2(aq)$ and pH results in Mg-silicate precipitation, we ran experiments varying Mg^{2+} concentrations (by 10 times over modern seawater) and at variable pH (Fig. 7). As discussed above, raising $SiO_2(aq)$ alone was insufficient to drive precipitation. In fact, our experiments identify pH as the primary control on Mg-silicate formation. At a pH_f of 8.0, we observed no precipitation over the course of the experiment. Within error, $SiO_2(aq)$ levels remained unchanged for > 5 months with no sign of precipitation. In contrast, the same Mg^{2+} and $SiO_2(aq)$ at elevated pH resulted in the rapid precipitation of Mg-silicate on the timescale of days, suggesting that despite exceedingly high Mg^{2+} levels, pH appears to be the primary control on Mg-silicate formation from seawater-derived solutions.

Solution chemistry at experiment termination tells a similar story. Relationships between $SiO_2(aq)$ loss and pH_f reveal a sharp speciation boundary for $SiO_2(aq)$ at ~8.6-8.7 (Fig. 8). Below this threshold, $SiO_2(aq)$ is unchanged within analytical error (compared to "blank" experiments conducted in the absence of $MgCl_2$). At $SiO_2(aq)$ concentrations between amorphous silica and quartz saturation, the dominant silica species in seawater is monomeric silica; $H_4SiO_4^0$. As pH is increased above ~8.5, $H_4SiO_4^0$ deprotonates, favoring $H_3SiO_4^-$ (Fig. 9).

As a result, at these higher pH values, the concentration of a Mg-silica complex ($MgH_3SiO_4^+$) increases sharply. The $MgH_3SiO_4^+$ species alone is probably not representative of all possible aqueous Mg-silica complexes in solution, especially given the complexity of silica speciation revealed by NMR (Felmy et al., 2001). Nevertheless, the stability constant for this species (derived from actual potentiometric measurements of SiO_2(aq) and Mg-bearing solutions at various pH and high salinity) shows that regardless of actual species distribution, the pH dependence of Mg-silica complexing is well represented by $MgH_3SiO_4^+$ (Santschi and Schindler, 1974).

It is possible that at low pH, the rate of crystallization is too slow to be observed. However, the idea of a minimum pH for Mg-silicate formation is well supported by previous synthesis experiments. For example, Siffert and Wey (1962), using dilute $MgCl_2$ solutions and monomeric SiO_2(aq), precipitated "true" sepiolite at pH >8.5. At pH >9, talc and stevensite formed. Abtahi (1985) and La Iglesia (1978) obtained similar results. The same trends have been observed by workers synthesizing "Mg-silicate hydrate" for industrial applications, with some citing a canonical pH for "Mg-silicate scale" formation of ~8.5 (Brew and Glasser, 2005a; Brew and Glasser, 2005b; Delacaillerie et al., 1995; Mizutani et al., 1990; Packter, 1986; Strese and Hofmann, 1941; Takahashi et al., 1994; Wei and Chen, 2006).

$MgH_3SiO_4^+$ and similar species are, in turn, the solution precursors to Mg-silicate precipitates (Packter, 1986). Theoretical treatments of layer silicate nucleation from solution require that an excess surface energy barrier be overcome by a critical supersaturation of a pre-existing solution complex (Carrado et al., 2006). The critical supersaturation barrier to initiate Mg-silicate formation, then, must occur close to pH 8.6-8.7. Below this point, speciation calculations show that aqueous Mg-silicate complexes, while present, are unlikely to be

368 concentrated enough to initiate the nucleation of a silicate phase; deprontonated silica species
369 would be kept to scant amounts in solution, preventing appreciable interaction with Mg^{2+}. This
370 strong kinetic control on Mg-silicate precipitation from seawater is reminiscent of the more
371 familiar problem of $CaCO_3$ precipitation from modern surface seawater. For both systems,
372 despite a clear thermodynamic driving force, a critical level of supersaturation is required. For
373 Mg-silicates, deprotonation of $H_4SiO_4^0$ at elevated pH appears to be the "switch" that enables
374 Mg-silica complexing, in turn driving Mg-silicate nucleation and precipitation.
375
376 *6.3 Burial diagenesis and turbostratic stacking disorder in talc*
377 The sedimentary record of authigenic Mg-silicates can be related to solution chemistry
378 only with knowledge of thermal transformations possible during burial diagenesis. Our
379 hydrothermal experiments run with poorly crystalline Mg-silicates precipitated from seawater
380 show that upon dehydration, the material readily transforms to kerolite. Previous work has
381 shown that with continued dehydration, either with time or at increased temperature, kerolite, in
382 turn, transforms to crystalline disordered talc (Mitsuda and Taguchi, 1977). Our heating
383 experiments with kerolite confirm these observations and show that the talc formed by
384 dehydrating kerolite exhibits severe layer stacking disorder identical to the disorder observed in
385 Akademikerbreen and Fifteenmile samples (Fig. 5).
386 Stacking disorder in talc is not uncommon. In fact, it results from an inherently weak
387 electrostatic charge between 2:1 layers (Giese, 1975). The disorder observed in our samples is
388 best matched by ordered stacking of 2:1 layers by $a/3$ along one of the pseudo-hexagonal axes,
389 with random displacements of $\pm b/3$ along another (Gualtieri, 1999). It is not clear why this type
390 of disordering results, but as others have noted, it may well be controlled by the pathway of

391 crystallization (in this case, dehydration) rather than solid state transformation (Baronnet, 1992;
392 Kogure and Kameda, 2008). Specifically, the 2:1 layer dehydration mechanism of the low
393 temperature precipitate, which initiates stacking to form kerolite and, in turn, talc, may well exert
394 the most control on the type of disorder that results from this pathway. Nevertheless, this poorly
395 understood feature is present in all Neoproterozoic samples, consistent with low temperature
396 precipitation and subsequent dehydration during burial.

397 Although there are no direct temperature constraints on the samples described herein,
398 Neoproterozoic strata in the Yukon are relatively low-grade for rocks of their age. Regionally,
399 conodont alteration indices and vitrinite reflectance from the overlying Paleozoic strata suggest
400 these rocks have not seen more than 140 ^{o}C (Van Kooten et al., 1997). A similar thermal history
401 of the Svalbard samples is suggested by paleomagnetic studies in which demagnetization
402 experiments removed a Caledonian thermochemical remnant magnetization at 150 ^{o}C (Maloof et
403 al., 2004). Moreover, the orange-brown color of preserved organic matter in the
404 Akademikerbreen Group indicates that the degree of graphitization and maximum burial
405 temperatures were modest. In reconciling these constraints with experimental data discussed
406 above, it is important to note that we have used elevated temperature (up to 400^{o}C) purely to
407 observe the dehydration of poorly crystalline Mg-silicate to kerolite and eventually to talc on
408 convenient laboratory timescales. However, this transition is known to occur in response to
409 lower temperature and longer reaction time (Mitsuda and Taguchi, 1977). Indeed, if the kinetics
410 of the Mg-silicate dehydration reaction were to behave in a similar fashion to other burial
411 diagenetic reactions involving clay minerals, the dehydration of poorly crystalline Mg-silicate to
412 talc could, for example, take as little as 10^5 years at ~80^{o}C (Velde, 1985).
413

414 *6.4 Mg-silicate formation on Neoproterozoic carbonate platforms*

415 Taken together, experimental data indicate that low temperature talc formation in
416 association with carbonates requires: (1) elevated SiO_2(aq), between quartz and amorphous silica
417 saturation; (2) sufficient (at least "modern") Mg^{2+}; (3) near marine salinity; (4) low Al (i.e., a
418 low background detrital flux, see below) and (5) elevated pH of at least ~8.7.

419 One key requirement for talc precipitation that we have yet to discuss is low Al, requiring
420 that detrital fluxes were low during deposition of the talc-bearing intervals in the
421 Akademikerbreen and Fifteenmile groups. As Al^{3+} increases in concentration, talc, a nominally
422 Al-free mineral, is no longer stable, being replaced instead by Al-bearing smectites, chlorites,
423 palygorskite or other minerals depending on local pore water chemistry and sediment supply
424 (Jones, 1986; Jones and Galan, 1988; Weaver and Beck, 1977). Low detrital fluxes have been
425 episodic features of carbonate platform environments throughout recorded Earth history, and
426 don't place a unique chemical constraint beyond that discussed. Thus, our mineralogical
427 observations of low siliciclastic flux in talc-bearing facies of the Akademikerbreen and
428 Fifteenmile successions helps to explain the distribution of early diagenetic talc in space but not
429 in time.

430 The requirement of elevated SiO_2(aq) concentration was also readily met in
431 Neoproterozoic seawater. Indeed, prior to the evolution of silica skeletons in sponges,
432 radiolarians and diatoms, Precambrian seawater should have carried higher silica concentrations
433 relative to modern levels (Maliva et al., 2005). Consistent with this expectation, early diagenetic
434 chert in Neoproterozoic carbonate successions, largely from peritidal or possibly mildly
435 evaporitic environments, provides evidence for local pore water enrichment in SiO_2(aq) on
436 shallow water platforms (Maliva et al., 2005). The Akademikerbreen Group abounds with

437 evidence for early diagenetic silicification (e.g., Fairchild et al. 1991; Knoll, 1984; Knoll and
438 Swett, 1990). Fifteenmile Group samples are also heavily silicified, but record a more complex
439 history of silicification (Mustard and Donaldson, 1990).

440 The Akademikerbreen and Fifteenmile Groups were likely deposited on marginal to
441 isolated marine platforms (Knoll and Swett, 1990; Macdonald et al., 2010). Near marine salinity
442 (~35‰) and Mg^{2+} concentrations are consistent with these settings, yet the salinity and Mg^{2+}
443 content of Proterozoic seawater is poorly constrained. Oolites in the Akademikerbreen Group
444 provide petrographic and geochemical (high Sr) evidence for an aragonite sea at the time of their
445 deposition, suggesting that contemporaneous seawater may have had Mg^{2+} concentrations
446 broadly similar to those observed today (Swett and Knoll, 1989). Although no evaporite minerals
447 or their associated pseudomorphs have been identified in either succession, episodic restriction in
448 the Akademikerbreen and Fifteenmile Groups cannot be ruled out. On the other hand, seawater
449 evaporation should *decrease* pH (e.g., McCaffrey et al., 1987), which is inconsistent with the
450 stability of talc.

451 Talc formation by meteoric mixing faces a similar constraint, as freshwater influx would
452 tend to drive pH below marine values. Additionally, salinity would further decrease in response
453 to post-depositional meteoric influx. Higher water activity (or lower salinity) favors the
454 precipitation of Mg-silicates of higher hydration, namely sepiolite. Lower water activity (or near
455 normal marine salinity), on the other hand, favors kerolite and/or other 2:1 silicates, and
456 synthesis work reinforces these constraints (Jones and Galan, 1988; Siffert and Wey, 1962;
457 Stoessell and Hay, 1978). Mg-silicate occurrences in peri-marine and lacustrine environments
458 also conform to this trend, so well, in fact, that Mg-silicate assemblages have been used to track
459 salinity fluctuations and the influence of meteoric water in a number of modern and ancient

460 settings (Calvo et al., 1999; Jones, 1986; Stoessell and Hay, 1978; Weaver and Beck, 1977;
461 Webster and Jones, 1994).

462 Of all the requirements for early diagenetic talc formation, elevated pH (≥ ~8.7) is the
463 most problematic, given the difficulty of increasing seawater pH, which is largely buffered by
464 the carbon cycle, to the required level. The more realistic alternative is to increase pH in pore
465 waters via microbial processes. Elevated pH can be achieved through certain microbial reactions
466 that remineralize organic matter, a set of processes that need not have decreased salinity, Mg^{2+}
467 and/or SiO_2(aq) levels. Both the Akademikerbreen and Fifteenmile talc deposits are intimately
468 associated with microbial facies: bedded talc drapes occur with microbialaminites and
469 stromatolites in Fifteenmile samples, and both localities host talc nodules within microbialites.

470 Anaerobic respiration is a particularly attractive mechanism for increasing pH. In a
471 Neoproterozoic world with low pO_2 and no macrometazoan bioturbation, anoxia would have
472 been a common feature of early diagenetic carbonate sediments. Given the additional likelihood
473 that nitrate levels were also low (Fennel et al., 2005), ferric iron and sulfate would have been the
474 most energetically favorable oxidants available for organic carbon remineralization, with Fe^{3+}
475 favored over SO_4^{2-} (Canfield et al., 2005). Under conditions where the reactive Fe flux was high,
476 (perhaps ultimately sourced from hydrothermal Fe fluxes rather than detrital input in these
477 sediment-starved environments) dissimilatory Fe reduction would have been particularly
478 effective at increasing pH through the following reaction:

479 $$2CH_2O + 8Fe(OH)_3 \rightarrow 2CO_2 + 8Fe^{2+} + 6H_2O + 16OH^-$$

480 When the reactive Fe pool was kept low, either by exhaustion of reactive Fe^{3+} or by pyrite
481 precipitation (Johnston et al., 2010; Lyons and Severmann, 2006), sulfate reduction would have
482 contributed to a pH increase in solution:

483 $$2CH_2O + SO_4^{2-} \rightarrow 2CO_2 + H_2S + 2OH^-$$

484 Fe-speciation and isotopic analyses of other early Neoproterozoic successions indicate that these
485 two metabolic pathways strongly influenced marine chemistry in both basinal and platform
486 settings, with organic carbon fluxes and variations in basinal Fe and S cycles controlling the
487 balance between them (Canfield et al., 2008; Johnston et al., 2010; Johnston et al., 2009). But
488 regardless of the interplay between different types of anaerobic respiration, both pathways would
489 have resulted in a pH increase without changes in other conditions needed for talc precipitation.
490 Pore waters in microbially-dominated sediments would have been especially susceptible to pH
491 increase driven by anaerobic respiration, where higher sediment to pore-water ratios favored
492 more effective changes in chemistry

493 In addition to the Svalbard and Canadian occurrences described here, sedimentary (oolitic)
494 talc has been reported in association with stromatolitic dolomites in an Infracambrian
495 (Neoproterzoic) succession of the Volta Basin of West Africa (Millot and Palausi, 1959). The
496 authors argue from petrographic analyses that talc formation preceded dolomitization and
497 silicification. Noack et al. (1989) also reported oolitic talc in the Schisto-Calcaire Group of the
498 West Congo Basin. Overlying the Upper Diamictite Formation, Schisto-Calcaire carbonates have
499 strontium isotope values of 0.7073 (Frimmel et al., 2006; Poidevin, 2007), consistent with a
500 Cryogenian age (716-635 Ma). The sedimentology of the Schisto-Calcaire Group has been
501 interpreted to reflect alternately shallow marine and lagoonal conditions, separated from outer
502 subtidal regions of the platform by stromatolitic reefs (Trompette and Boudzoumou, 1988).
503 Noack et al. (1989) interpret the talc to have formed by transformation from stevensite or
504 sepiolite on the basis of thermodynamic considerations. This interpretation is not incompatible
505 with ours; stevensite precipitation is generally only observed from synthesis studies at high pH

and near marine salinity (La Iglesia, 1978; Siffert and Wey, 1962). We have not conclusively identified stevensite in our experiments, but have identified a corrensite-like phase forming with talc at high pH. Corrensite formation at low temperature requires the initial formation of a stevensite-like smectite into which brucite-like layers are precipitated (Reynolds, 1988).

The apparent concentration of low temperature talc deposits in mid-Neoproterozic carbonate platforms may find explanation in the superposition of Neoproterozoic-specific environmental conditions on the broader set of requirements (low detrital influx, high silica, low oxygen, sufficient Mg, efficient sulfide scavenging (Ben-Yaakov, 1973)) likely to have characterized Precambrian carbonate platforms in general. Fe speciation chemistry indicates that iron played a more important role in organic remineralization after 800 million years ago than it did earlier in the Proterozoic Eon (Canfield et al., 2008; Johnston et al., 2010). Also, the hypothesized shift from a Mesoproterozoic biosphere with warm, high pCO_2 atmosphere with high seawater DIC to a more glacial-prone later Neoproterozoic world with lower pCO_2 and DIC would further have eased chemical resistance to increases in pore-water pH in Neoproterozoic carbonate platforms (Kah and Bartley, 2004). During deposition of the Akademikerbreen and Fifteenmile Groups, anaerobic respiration in microbial sediment receiving little terrigenous input provided a fortuitous combination of chemistry and depositional conditions to increase pH and precipitate authigenic Mg-silicate at near marine salinity. The subsequent burial of this material would have driven a thermal transformation to kerolite and eventually to turbostratically-disordered talc.

Talc is not the only product to result from unusual pore water chemistry on Neoproterozoic platforms. As discussed above, the identification of saponite, an Al-bearing trioctahedral smectite, suggests additional diagenetic reactions. In the absence of kinetic

529 constraints, but instead using thermodynamic considerations based on field data, Weaver and
530 Beck (1977) suggest modern seawater need only increased SiO_2(aq) and/or pH to drive a
531 diagenetic conversion from detrital montmorillonite to saponite. Thus, the same chemical
532 conditions that led to talc precipitation were also capable of driving smectite recrystallization.
533 Bristow et al. (2009) identified saponite (and corrensite) in Member 2 of the Ediacaran
534 Doushantuo Formation and suggested a lacustrine depositional environment. Our data, however,
535 show that early diagenetic modification of Neoproterozoic seawater is also capable of producing
536 saponite. Thus, in the absence of independent sedimentological evidence of non-marine
537 deposition, saponite cannot be taken as evidence for lacustrine deposition in Neoproterozoic
538 successions. Indeed, the common occurrence of saponite in modern lacustrine settings rather than
539 marine may simply reflect decreased seawater silica levels after the radiation of siliceous
540 plankton in addition to lower modern marine pH. This evolutionary innovation alone would have
541 been sufficient to leave modern saline lakes among the few environments able to concentrate and
542 drive saponite formation from a dioctahedral precursor.
543
544 **7. Conclusions**
545 Sedimentology, petrography and mineralogy all indicate that sedimentary talc reflects
546 distinct aqueous chemistry recorded on two separate Neoproterozoic carbonate platform margins.
547 Precipitation experiments with modified "Neoproterozoic-like" seawater show that elevated
548 SiO_2(aq), normal marine salinity and Mg^{2+} levels, and low Al^{3+} all favor talc formation. However,
549 the switch that enables talc nucleation is elevated pH. Above pH 8.6-8.7, the deprotonation of
550 $H_4SiO_4^0$ initiates Mg-silica complexation and nucleation, which leads to the subsequent
551 formation of a kerolite precursor composed of hydrated 2:1 layers with little to no stacking order.

552 The progressive dehydration of this material, driven by low water activity in solution or by burial
553 diagenesis, leads to the formation of kerolite and eventually turbostratic talc.

554 Our analyses, together with other reports of sedimentary talc through this interval,
555 suggest that the later Neoproterozoic Era seawater unusually favorable for early diagenetic talc
556 precipitation. Although we argue that talc precipitation was occurring within the sediment,
557 contemporaneous seawater must have been specially poised, only requiring reasonable changes
558 to chemistry within the pore-waters. Following from this, we suggest that anaerobic respiration
559 may have provided the alkalinity pump that tipped the scales toward talc formation in soft
560 sediments. The degree to which sedimentary processes altered overlying seawater, neither of
561 which are known uniquely, hinders direct interpretation of paleo-seawater compositions and pH.
562 Further, whether the Neoproterozoic was the first and last time talc formed with marine
563 carbonates at low temperature is unclear, but its identification of multiple continents speaks to
564 the state of the Cryogenian oceans. This study does elucidate that insight into seawater and pore-
565 water chemistry is clearly recorded by early diagenetic Mg-silicates. An improved understanding
566 of the kinetic and thermodynamic controls behind their formation will continue to exploit these
567 minerals as recorders of early diagenetic chemistry in modern and ancient marine and lacustrine
568 settings.

569

570 **Acknowledgements**

571 NJT acknowledges support from Royal Society Research Grant 2009/R2 and from Churchill
572 College, Cambridge. NJT also thanks T. Abraham, M. Zhang, R. Harrison, R. Parsons and M.
573 Walker for analytical assistance, and C. Jeans for fruitful discussions. Research by AHK and
574 DTJ supported, in part, by NASA Exobiology grant NNX07AV51G. FAM and JVS thank

575 Charlie Roots and the Yukon Geological Survey for logistical support. The authors thank David
576 Fike for constructive reviews.
577

578 **References**

579 Abbott, G., 1997, Geology of the Upper Hart River Area, Eastern Ogilvie Mountains, Yukon
580 Territory (116A/10, 116A/11): Exploration and Geological Services Division, Yukon
581 Region, Bulletin, v. 9, p. 1-76.

582 Abtahi, A., 1985, Synthesis of sepiolite at room-temperature from SiO_2 and $MgCl_2$ Solution:
583 Clay Minerals, v. 20, p. 521-523.

584 Baronnet, A., 1992, Polytypism and stacking disorder, *in* Buseck, P.R., ed., Minerals and
585 reactions at the atomic scale: Transmission electron microscopy, Volume 27: Washington,
586 DC, Mineralogical Society of America, p. 231-288.

587 Ben-Yaakov, S., 1973, pH buffering of pore water of recent anoxic marine sediments: Limnol.
588 Oceanogr., v. 18, p. 86-94.

589 Bodine, M.W., 1983, Trioctahedral clay mineral assemblages in Paleozoic marine evaporite
590 rocks, Sixth International Symposium on Salt, Volume 1, Salt Institute, p. 267-284.

591 Braitsch, O., 1971, Salt Deposits, Their Origin and Composition: Berlin, Springer-Verlag.

592 Brew, D.M.R., and Glasser, F.P., 2005a, The magnesia-silica gel phase in slag cements: alkali (K,
593 Cs) sorption potential of synthetic gels: Cement and Concrete Research, v. 35, p. 77-83.

594 Brew, D.R.M., and Glasser, F.P., 2005b, Synthesis and characterisation of magnesium silicate
595 hydrate gels: Cement and Concrete Research, v. 35, p. 85-98.

596 Brindley, G.W., Bish, D.L., and Wan, H.M., 1977, Nature of kerolite and its relation to talc and
597 stevensite: Mineralogical Magazine, v. 41, p. 443-452.

598 Bristow, T.F., Kennedy, M.J., Derkowski, A., Droser, M.L., Jiang, G.Q., and Creaser, R.A., 2009,
599 Mineralogical constraints on the paleoenvironments of the Ediacaran Doushantuo
600 Formation: Proceedings of the National Academy of Sciences of the United States of
601 America, v. 106, p. 13190-13195.
602 Butterfield, N.J., Knoll, A.H., and Swett, K., 1994, Paleobiology of the Neoproterozoic
603 Svanbergfjellet Formation, Spitsbergen: Fossils and Strata, v. 34, p. 1-84.
604 Calvo, J.P., Blanc-Valleron, M.M., Rodriguez-Arandia, J.P., Rouchy, J.M., and Sanz, M.E., 1999,
605 Authigenic clay minerals in continental evaporitic environments, Special Publication IAS,
606 Volume 27, IAS, p. 129-151.
607 Canfield, D.E., Kristensen, E., and Thamdrup, B., 2005, Aquatic Geomicrobiology: Amsterdam,
608 Elsevier, 636 p.
609 Canfield, D.E., Poulton, S.W., Knoll, A.H., Narbonne, G.M., Ross, G., Goldberg, T., and Strauss,
610 H., 2008, Ferruginous conditions dominated later neoproterozoic deep-water chemistry:
611 Science, v. 321, p. 949-952.
612 Carrado, K.A., Decarreau, A., Petit, S., Bergaya, F., and Lagaly, G., 2006, Synthetic clay
613 minerals and purification of natural clays, *in* Bergaya, F., Theng, B.K.G., and Lagaly, G.,
614 eds., Handbook of Clay Science, Volume 1, Elsevier, p. 115-139.
615 Delacaillerie, J.B.D., Kermarec, M., and Clause, O., 1995, Si-29 NMR Observation of an
616 amorphous magnesium-silicate formed during impregnation of silica with Mg(II) in
617 aqueous-solution: Journal of Physical Chemistry, v. 99, p. 17273-17281.
618 Derry, L.A., Keto, L.S., Jacobsen, S.B., Knoll, A.H., and Swett, K., 1989, Sr isotopic variations
619 in Upper Proterozoic carbonates from Svalbard and East Greenland: Geochimica et
620 Cosmochimica Acta, v. 53, p. 2231-2239.

621 Dietzel, M., 2000, Dissolution of silicates and the stability of polysilicic acid: Geochimica et
622 Cosmochimica Acta, v. 64, p. 3275-3281.
623 Evans, B.W., and Guggenheim, S., 1988, Talc, Pyrophyllite, and Related Minerals: Reviews in
624 Mineralogy, v. 19, p. 225-294.
625 Fairchild, I.J., Knoll, A.H., and Swett, K., 1991, Coastal lithofacies and biofacies associated with
626 syndepositional dolomitization and silicification (Draken Formation, Upper Riphean,
627 Svalbard): Precambrian Research, v. 53, p. 165-197.
628 Farmer, V.C., 1974, The layer silicates, *in* Farmer, V.C., ed., The Infrared Spectra of Minerals:
629 Mineralogical Society Monograph: London, Mineralogical Society, p. 331-364.
630 Felmy, A.R., Cho, H., Rustad, J.R., and Mason, M.J., 2001, An aqueous thermodynamic model
631 for polymerized silica species to high ionic strength: Journal of Solution Chemistry, v. 30,
632 p. 509-525.
633 Fennel, K., Follows, M., and Falkowski, P.G., 2005, The co-evolution of the nitrogen, carbon
634 and oxygen cycles in the Proterozoic ocean: American Journal of Science, v. 305, p. 526-
635 545.
636 Friedman, G.M., 1965, Occurrence of talc as a clay mineral in sedimentary rocks: Nature, v. 207,
637 p. 283-284.
638 Frimmel, H.E., Tack, L., Basel, M.S., Nutman, A.P., and Boven, A., 2006, Provenance and
639 chemostratigraphy of the Neoproterozoic West Congolian Group in the Democratic
640 Republic of Congo: Journal of African Earth Sciences, v. 46, p. 221-239.
641 Giese, R.F., 1975, Interlayer bonding in talc and pyrophyllite: Clays and Clay Minerals, v. 23, p.
642 165-166.

643 Gualtieri, A.F., 1999, Modelling the nature of disorder in talc by simulation of X-ray powder
644 patterns: European Journal of Mineralogy, v. 11, p. 521-532.
645 Halverson, G.P., Dudas, F.O., Maloof, A.C., and Bowring, S.A., 2007, Evolution of the Sr-87/Sr-
646 86 composition of Neoproterozoic seawater: Palaeogeography Palaeoclimatology
647 Palaeoecology, v. 256, p. 103-129.
648 Iler, R.K., 1979, The Chemistry of Silica: Solubility, Polymerization, Colloid and Surface
649 Properties, and Biochemistry: New York, Wiley, 866 p.
650 Jefferson, C.W., and Parrish, R., 1989, Late Proterozoic stratigraphy, U/Pb zircon ages and rift
651 tectonics, Mackenzie Mountains, northwestern Canada: Canadian Journal of Earth
652 Sciences, v. 26, p. 1784-1801.
653 Johnston, D.T., Poulton, S.W., Dehler, C., Porter, S., Husson, J., Canfield, D.E., and Knoll, A.H.,
654 2010, An emerging picture of Neoproterozoic ocean chemistry: Insights from the Chuar
655 Group, Grand Canyon, USA: Earth and Planetary Science Letters, v. 290, p. 64-73.
656 Johnston, D.T., Wolfe-Simon, F., Pearson, A., and Knoll, A.H., 2009, Anoxygenic
657 photosynthesis modulated Proterozoic oxygen and sustained Earth's middle age:
658 Proceedings of the National Academy of Sciences of the United States of America, v. 106,
659 p. 16925-16929.
660 Jones, B.F., 1986, Clay mineral diagenesis in lacustrine sediments, *in* Mumpton, F.A., ed.,
661 Studies in Diagenesis, Volume 1578: USGS Bulletin, U.S. Geological Survey, p. 291-300.
662 Jones, B.F., and Galan, E., 1988, Sepiolite and Palygorskite: Reviews in Mineralogy, v. 19, p.
663 631-674.
664 Kah, L.C., and Bartley, J.K., 2004, Marine carbon reservoir, C-org-C-carb coupling, and the
665 evolution of the Proterozoic carbon cycle: Geology, v. 32, p. 129-132.

666 Knoll, A.H., 1984, Microbiotas of the Late Precambrian Hunnberg Formation, Nordaustlandet,
667 Svalbard: Journal of Paleontology, v. 58, p. 131-162.
668 Knoll, A.H., Hayes, J.M., Kaufman, A.J., Swett, K., and Lambert, I.B., 1986, Secular variation in
669 carbon isotope ratios from Upper Proterozoic successions of Svalbard and East
670 Greenland: Nature, v. 321, p. 832-838.
671 Knoll, A.H., and Swett, K., 1990, Carbonate deposition during the Late Proterozoic Era - an
672 example from Spitsbergen: American Journal of Science, v. 290A, p. 104-132.
673 Kogure, T., and Kameda, J., 2008, High-resolution TEM and XRD simulation of stacking
674 disorder in 2 : 1 phyllosilicates: Zeitschrift Fur Kristallographie, v. 223, p. 69-75.
675 La Iglesia, A., 1978, Sintesis de la sepiolita a temperatura ambiente por precipitacion homogenea:
676 Boletin Geologico Minero, v. 89, p. 258-265.
677 Lyons, T.W., and Severmann, S., 2006, A critical look at iron paleoredox proxies: New insights
678 from modern euxinic marine basins: Geochimica Et Cosmochimica Acta, v. 70, p. 5698-
679 5722.
680 Macdonald, F.A., and Roots, C.F., 2009, Upper Fifteenmile Group in the Ogilvie Mountains and
681 correlations of early Neoproterozoic strata in the nothern Cordillera, *in* McFarlane, K.E.,
682 Weston, L.H., and Blackburn, L.R., eds., Yukon Exploration and Geology 2009:
683 Whitehorse, YT, Yukon Geological Survey, p. 237-252.
684 Macdonald, F.A., Schmitz, M.D., Crowley, J.L., Roots, C.F., Jones, D.S., Maloof, A.C., Strauss,
685 J.V., Cohen, P.A., Johnston, D.T., and Schrag, D.P., 2010, Calibrating the Cryogenian:
686 Science, v. 327, p. 1241-1243.

687 Maliva, R.G., Knoll, A.H., and Simonson, B.M., 2005, Secular change in the Precambrian silica
688 cycle: Insights from chert petrology: Geological Society of America Bulletin, v. 117, p.
689 835-845.
690 Maloof, A.C., Halverson, G.P., Kirschvink, J.L., Hoffman, P.F., and Schrag, D.P., 2004, Inertial
691 interchange true polar wander: combined paleomagnetic, isotopic and stratigraphic
692 evidence from the Neoproterozoic Akademikerbreen Group, Svalbard: Geological
693 Society of America Bulletin, v. 118, p. 1099-1124.
694 Marumo, K., and Hattori, K.H., 1999, Seafloor hydrothermal clay alteration at Jade in the back-
695 arc Okinawa Trough: Mineralogy, geochemistry and isotope characteristics: Geochimica
696 Et Cosmochimica Acta, v. 63, p. 2785-2804.
697 McCaffrey, M.A., Lazar, B., and Holland, H.D., 1987, The evaporation path of seawater and the
698 coprecipitation of Br^- and K^+ with halite: Journal of Sedimentary Petrology, v. 57, p. 928-
699 937.
700 Millot, G., and Palausi, G., 1959, Sur un talc d'origine sedimentaire: Comptes Rendus Societe
701 Geologique Francais, p. 45-47.
702 Mitsuda, T., and Taguchi, H., 1977, Formation of magnesium-silicate hydrate and its
703 crystallization to talc: Cement and Concrete Research, v. 7, p. 223-230.
704 Mizutani, T., Fukushima, Y., and Kamigaito, O., 1990, Mechanism of the copolymerization of
705 silicic-acid and metal-ions in aqueous-media: Bulletin of the Chemical Society of Japan,
706 v. 63, p. 618-619.
707 Mustard, P.S., and Donaldson, J.A., 1990, Paleokarst breccias, calcretes, silcretes and fault talus
708 breccias at the base of upper Proterozoic "Windermere" strata, northern Canadian
709 Cordillera: Journal of Sedimentary Petrology, v. 60, p. 525-539.

710 Noack, Y., Decarreau, A., Boudzoumou, F., and Trompette, R., 1989, Low-temperature oolitic
711 talc in Upper Proterozoic rocks, Congo: Journal of Sedimentary Petrology, v. 59, p. 717-
712 723.
713 Packter, A., 1986, Precipitation of alkaline-earth metal silicate hydrates from aqueous solution -
714 Ionic equilibria, crystalline phases and precipitation mechanisms: Crystal Research and
715 Technology, v. 21, p. 575-585.
716 Poidevin, J.L., 2007, Sr-isotope stratigraphy and dating of Neoproterozoic carbonates and
717 glacials from the northern and western parts of the Congo Craton: Comptes Rendus
718 Geoscience, v. 339, p. 259-273.
719 Reynolds Jr., R.C., 1988, Mixed layer chlorite minerals, *in* Bailey, S.W., ed., Hydrous
720 Phyllosilicates, Volume 19: Washington, DC, Mineralogical Society of America, p. 725.
721 Russell, J.D., and Fraser, A.R., 1994, Infrared methods, *in* Wilson, M.J., ed., Clay Mineralogy:
722 Spectroscopic and Chemical Determinative Methods: London, Chapman and Hall, p. 11-
723 67.
724 Santschi, P.H., and Schindler, P., 1974, Complex-Formation in Ternary-Systems Ca(II)-H_4SiO_4-
725 H_2O and Mg(II)-H_4SiO_4-H_2O: Journal of the Chemical Society-Dalton Transactions, p.
726 181-184.
727 Siffert, B., and Wey, R., 1962, Synthese d'une sepiolite a temperature ordinaire: Comptes
728 Rendus de l'Academie des Sciences, v. 253, p. 142-145.
729 Stoessell, R.K., and Hay, R.L., 1978, Geochemical origin of sepiolite and kerolite at Amboseli,
730 Kenya: Contributions to Mineralogy and Petrology, v. 65, p. 255-267.

731 Strese, H., and Hofmann, U., 1941, Synthese von Magnesiumsilikat-Gelen mit zweidimensional
732 regelmaessiger struktur: Zeitschrift fur Anorganische und Allgemeine Chemie, v. 247, p.
733 65-95.
734 Swett, K., and Knoll, A.H., 1989, Marine pisolites from Upper Proterozoic Carbonates of East
735 Greenland and Spitsbergen: Sedimentology, v. 36, p. 75-93.
736 Takahashi, N., Tanaka, M., Satoh, T., and Endo, T., 1994, Study of synthetic clay-minerals .3.
737 Synthesis and characterization of 2-dimensional talc: Bulletin of the Chemical Society of
738 Japan, v. 67, p. 2463-2467.
739 Trompette, R., and Boudzoumou, F., 1988, Paleogeographic significance of stromatolitic
740 buildings on late Proterozoic platforms: The example of the West Congo Basin:
741 Palaeogeography Palaeoclimatology Palaeoecology, v. 48, p. 101-112.
742 Turner, E.C., and Long, D.G.F., 2008, Basin architecture and syndepositional fault activity
743 during deposition of the Neoproterozoic Mackenzie Mountains Supergroup, Northwest
744 Territories, Canada: Canadian Journal of Earth Sciences, v. 45, p. 1159-1184.
745 Van Kooten, G.K., Watts, A.B., Coogan, J., Mount, V.S., Swenson, R.F., Daggett, P.H., Clough,
746 J.G., Roberts, C.T., and Bergman, S.C., 1997, Alaska Division of Geological and
747 Geophysical Surveys, Report of Investigations 96-6A: Fairbanks, AK.
748 Velde, B., 1985, Clay Minerals: A Physico-Chemical Explanation of their Occurrence:
749 Amsterdam, Elsevier, 427 p.
750 Velde, B., and Meunier, A., 2008, The Origin of Clay Minerals in Soils and Weathered Rocks:
751 Berlin, Springer-Verlag, 406 p.
752 Weaver, C.E., and Beck, K.C., 1977, Miocene of SE United-States - Model for chemical
753 sedimentation in a peri-marine environment: Sedimentary Geology, v. 17, p. 1-234.

754 Webster, D.M., and Jones, B.F., 1994, Paleoenvironmental implications of lacustrine clay
755 minerals from the Double Lakes Formation, Southern High Plains, Texas, Sedimentology
756 and Geochemistry of Modern and Ancient Saline Lakes, Volume 50: SEPM Special
757 Publication, SEPM, p. 159-172.
758 Wei, J.X., and Chen, Y.M., 2006, Research on the cementious materials in MgO-SiO_2-H_2O
759 system at room temperature, *in* Tongbo, S., Rongxi, S., and Wensheng, Z., eds.,
760 Proceedings of the 6th International Symposium on Cement & Concrete and
761 CANMET/ACI International Symposium on Concrete Technology for Sustainable
762 Development, Vols 1 and 2, p. 594-598.
763 Wollast, R., Mackenzie, F.T., and Bricker, O.P., 1968, Experimental precipitation and genesis of
764 sepiolite at Earth-surface conditions: American Mineralogist, v. 53, p. 1645-1661.
765 Zhang, M., Hui, Q., Lou, X.-J., Redfern, S.A.T., Salje, E.K.H., and Tarantino, S.C., 2006,
766 Dehydroxylation, proton migration, and structural changes in heated talc: An infrared
767 spectroscopic study: American Mineralogist, v. 91, p. 816-825.
768
769 **Figure captions**
770 **Figure 1.** Bedded and nodular talc interbedded with microbialite in the Callison Lake Dolostone,
771 Ogilvie Mountains, Yukon.
772
773 **Figure 2.** Stratigraphic sections of the Fifteenmile and Akademikerbreen talc-bearing deposits.
774

775 **Figure 3.** Void-filling talc nodules (in outcrop (A) and thin section (B) under cross-polarized
776 light) formed in dolomitic stromatolite of the Hunnberg Fm, Nordaustlandet, Svalbard. The talc
777 in (B) (orange-brown) appears penecontemporaneous with void-filling microspar cement.
778
779 **Figure 4.** XRD patterns of oriented aggregates of the <2μm fraction extracted from talc-bearing
780 rocks. Black lines indicate scans acquired in the air-dried (Ca-saturated) state and red lines
781 indicate scans acquired in the EG-solvated state. (A) Talc from unit PF2 (U. Fifteenmile Group;
782 F927-58m) (B) Talc, saponite, and chlorite/smectite from the Hunnberg Fm (K2016). (C)
783 Saponite and illite/smectite from the Hunnberg Fm (HU1246). (D) Trioctahedral low-charge
784 corrensite from the Svanbergfjellet Fm (86-G-3).
785
786 **Figure 5.** Representative powder XRD patterns of randomly-oriented experimental precipitates
787 formed by (A) low temperature precipitation from modified seawater, (B) heating a low
788 temperature precipitate at 180^{o}C for 4 weeks, (C) heating the precipitate from (B) at 400^{o}C for 4
789 days. For comparison, a cleaned talc nodule from the Svanbergfjellet Fm is shown (D),
790 indicating extensive layer stacking disorder. “C” = cristobalite; “D” = dolomite.
791
792 **Figure 6.** FT-IR spectra of experimental Mg-silicate precipitates (black) in comparison to talc
793 collected from the Svanbergfjellet Fm (red). (A) Lattice vibration region, (B) Si-O stretching
794 region, (C) H_2O and CO_3 region, (D) OH stretching region.
795
796 **Figure 7.** Solubility diagram showing the equilibrium solubilities of crystalline talc (Jones,
797 1986), kerolite and sepiolite (Jones and Galan, 1988), “amorphous sepiolite” from Wollast et al.

798 (1968) and the equilibrium boundary between montmorillonite and saponite from Weaver and
799 Beck (1978). Data points represent *apparent solubilities* calculated from solutions collected upon
800 experiment termination. Experiments that have resulted in Mg-silicate precipitate form an
801 apparent boundary approximately parallel to kerolite and/or sepioilite, but these data do not
802 represent true equilibrium conditions with respect to either of these crystalline phases. Green
803 point represents experiment at elevated Mg and pH_f = 8.0 where no precipitate formed.
804
805 **Figure 8.** SiO_2(aq) loss as a function of final pH showing the sharp pH control on Mg-silicate
806 precipitation. Process blank experiments conducted with no $MgCl_2$(aq) indicate that one
807 experiment (pH_f ~9.2) has resulted in SiO_2(aq) loss that cannot be explained by experimental
808 artifacts alone and suggests the formation of a precipitate that was unable to be extracted for
809 analysis.
810
811 **Figure 9.** Thermodynamic calculations of SiO_2(aq) species distribution in "Neoproterozoic-like"
812 seawater as a function of pH. The sharp pH control on the $MgH_3SiO_4^+$ species represents the
813 effect of pH on potential nucleation of Mg-silicate from seawater at elevated SiO_2(aq). Initial
814 SiO_2(aq) = 60 mg/kg and initial SO_{4T} = 2.8 mmol/kg. Charge balance was satisfied by
815 readjustment of CO_2-HCO_3-CO_3 equilibria in an open system with respect to CO_2(g). All mineral
816 precipitation was suppressed.

Figure 1.

Figure 2.

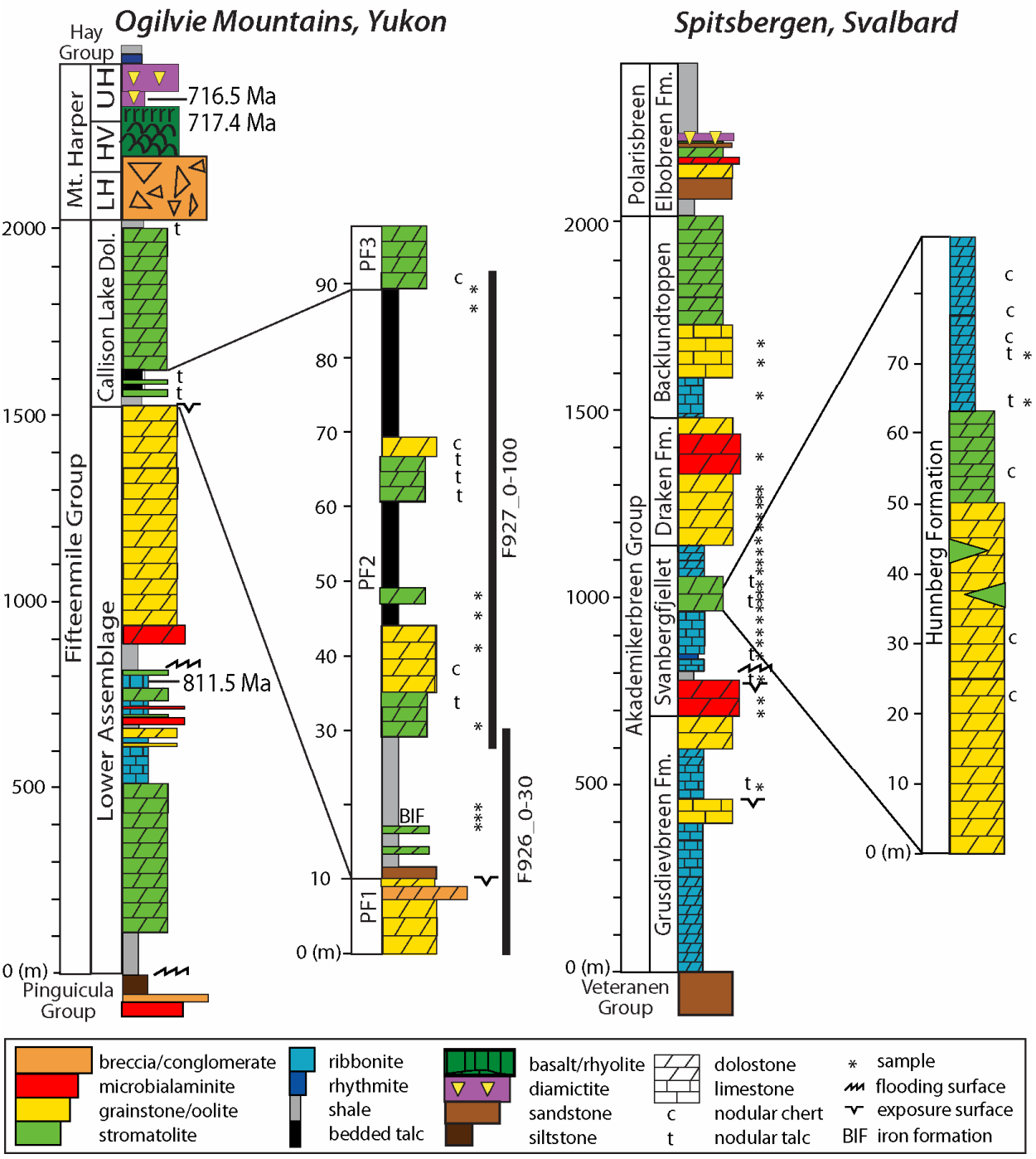
Ogilvie Mountains, Yukon
Spitsbergen, Svalbard
Hay Group
Mt. Harper
UH
HV
LH
716.5 Ma
717.4 Ma
Callison Lake Dol.
Fifteenmile Group
Lower Assemblage
811.5 Ma
Pinguicula Group
PF3
PF2
PF1
BIF
F927_0-100
F926_0-30
Polarisbreen
Elbobreen Fm.
Backlundtoppen
Draken Fm.
Akademikerbreen Group
Svanbergfjellet
Grusdievbreen Fm.
Hunnberg Formation
Veteranen Group
2000
1500
1000
500
0 (m)
90
80
70
60
50
40
30
10
breccia/conglomerate
microbialaminite
grainstone/oolite
stromatolite
ribbonite
rhythmite
shale
bedded talc
basalt/rhyolite
diamictite
sandstone
siltstone
dolostone
limestone
nodular chert
nodular talc
sample
flooding surface
exposure surface
iron formation

Figure 3.

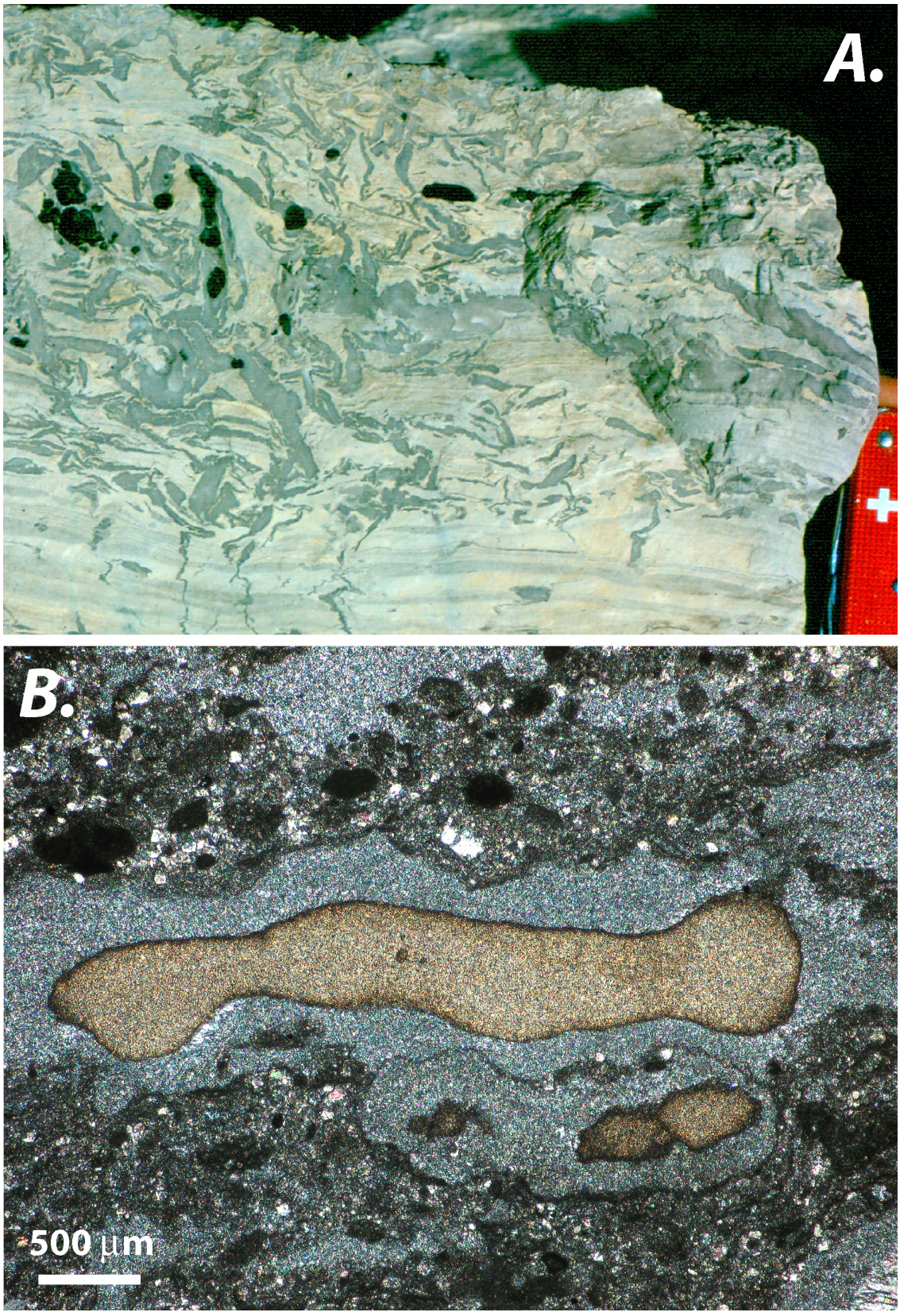

Figure 4.

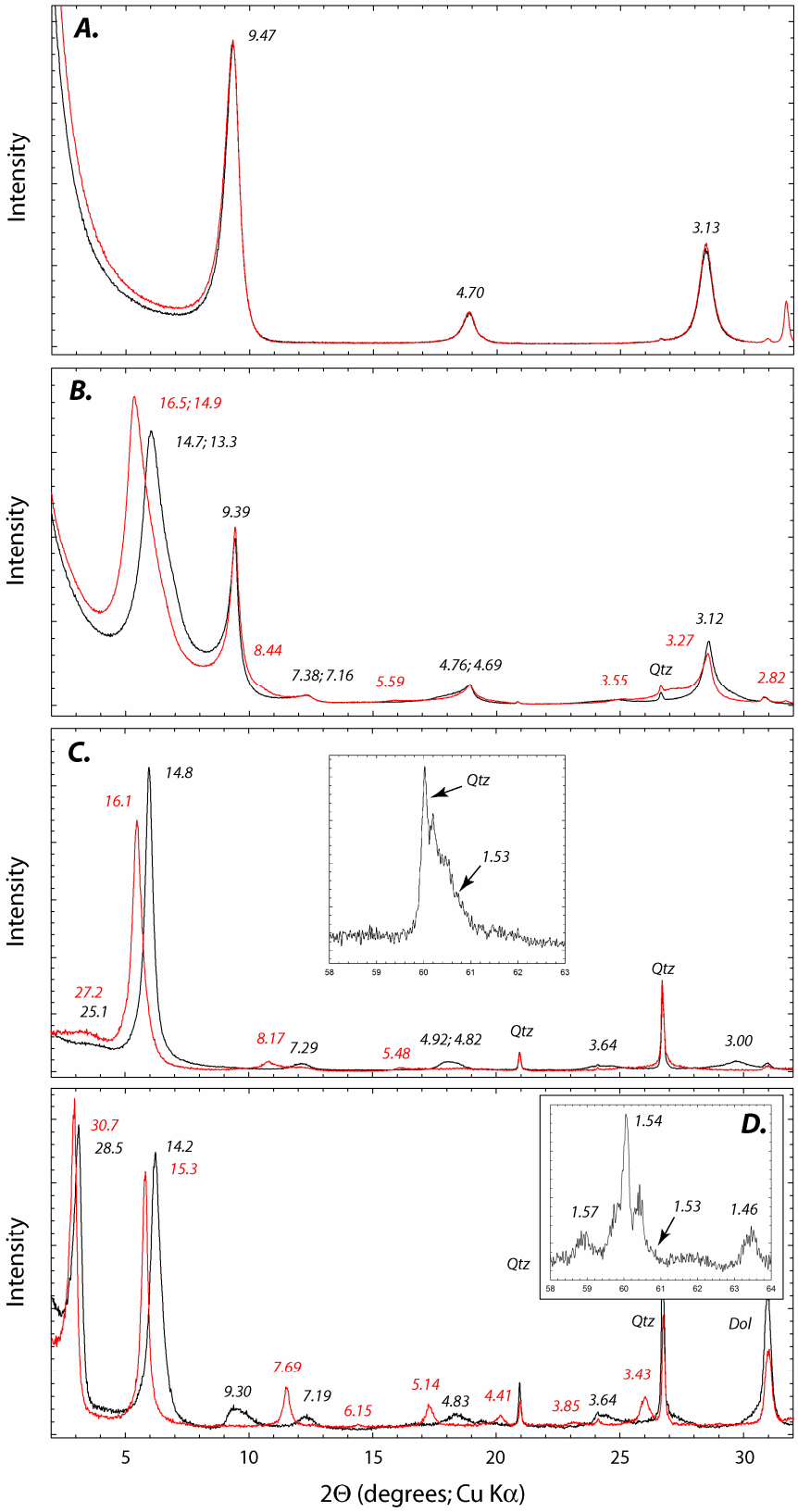
A.
9.47
4.70
3.13
Intensity
B.
16.5; 14.9
14.7; 13.3
9.39
8.44
7.38; 7.16
5.59
4.76; 4.69
3.55
Qtz
3.27
3.12
2.82
Intensity
C.
14.8
16.1
27.2
25.1
8.17
7.29
5.48
4.92; 4.82
Qtz
3.64
Qtz
3.00
1.53
58
59
60
61
62
63
Intensity
D.
30.7
28.5
14.2
15.3
9.30
7.69
7.19
6.15
5.14
4.83
4.41
3.85
3.64
3.43
Qtz
Dol
1.54
1.57
1.53
1.46
58
59
60
61
62
63
64
Intensity
5
10
15
20
25
30
2Θ (degrees; Cu Kα)

Figure 5.

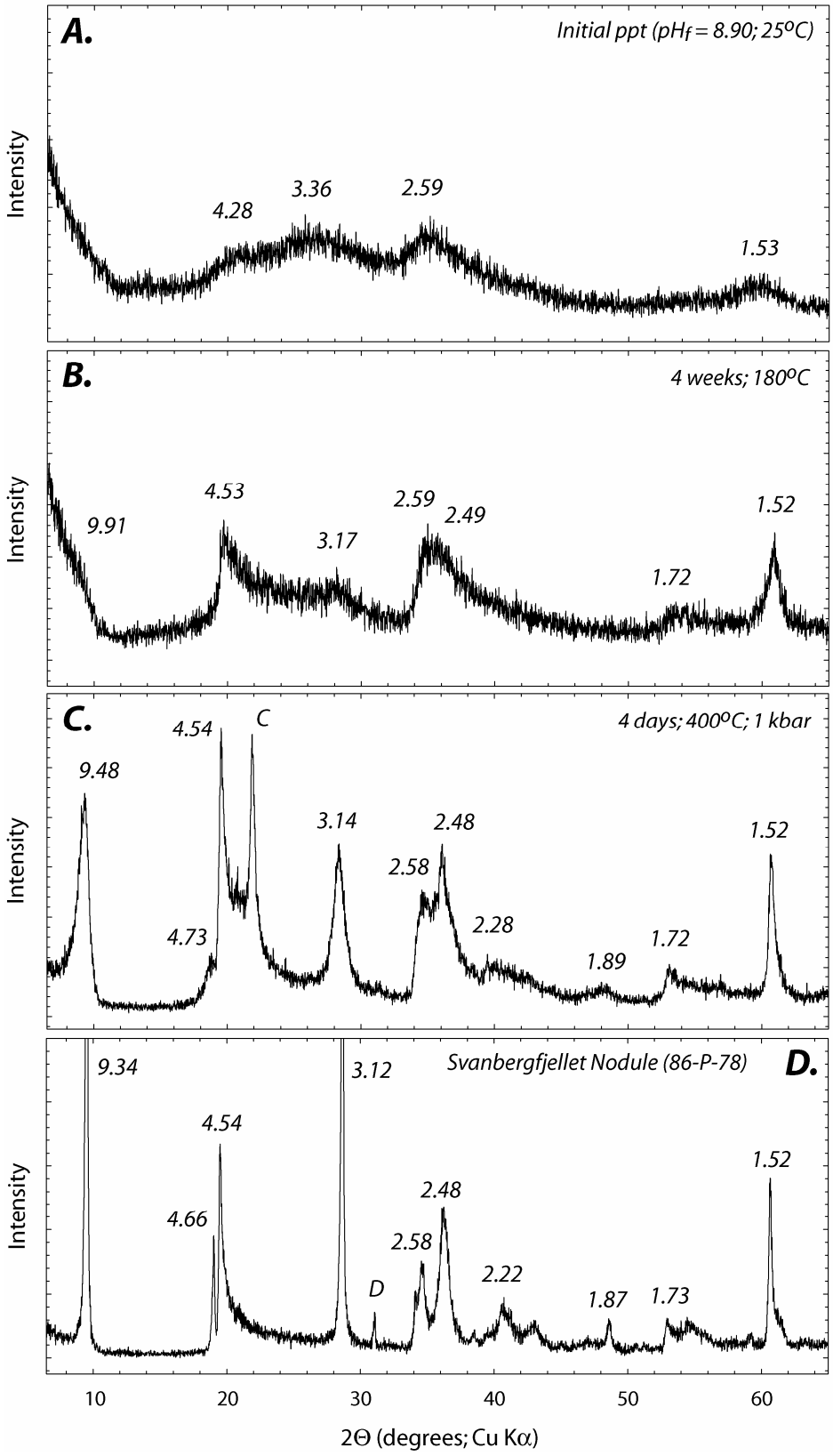
A.
Initial ppt (pHf = 8.90; 25°C)
4.28
3.36
2.59
1.53
B.
4 weeks; 180°C
9.91
4.53
3.17
2.59
2.49
1.72
1.52
C.
4 days; 400°C; 1 kbar
9.48
4.54
C
4.73
3.14
2.58
2.48
2.28
1.89
1.72
1.52
D.
Svanbergfjellet Nodule (86-P-78)
9.34
4.54
4.66
3.12
D
2.58
2.48
2.22
1.87
1.73
1.52
Intensity
10
20
30
40
50
60
2Θ (degrees; Cu Kα)

Figure 6.

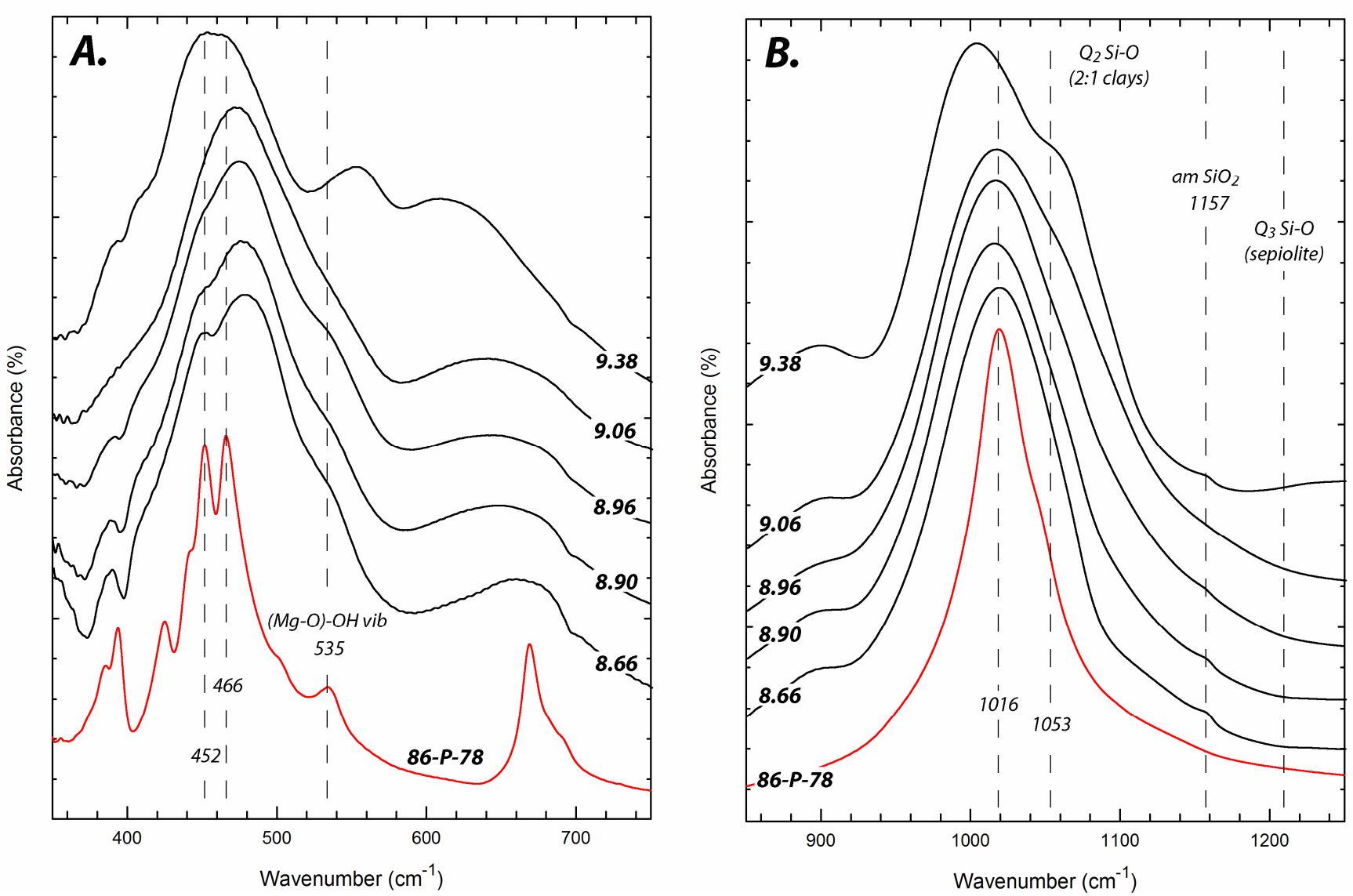
A.
Absorbance (%)
9.38
9.06
8.96
8.90
8.66
(Mg-O)-OH vib
535
466
452
86-P-78
400
500
600
700
Wavenumber (cm-1)
B.
Q2 Si-O
(2:1 clays)
am SiO2
1157
Q3 Si-O
(sepiolite)
9.38
9.06
8.96
8.90
8.66
1016
1053
86-P-78
900
1000
1100
1200
Wavenumber (cm-1)

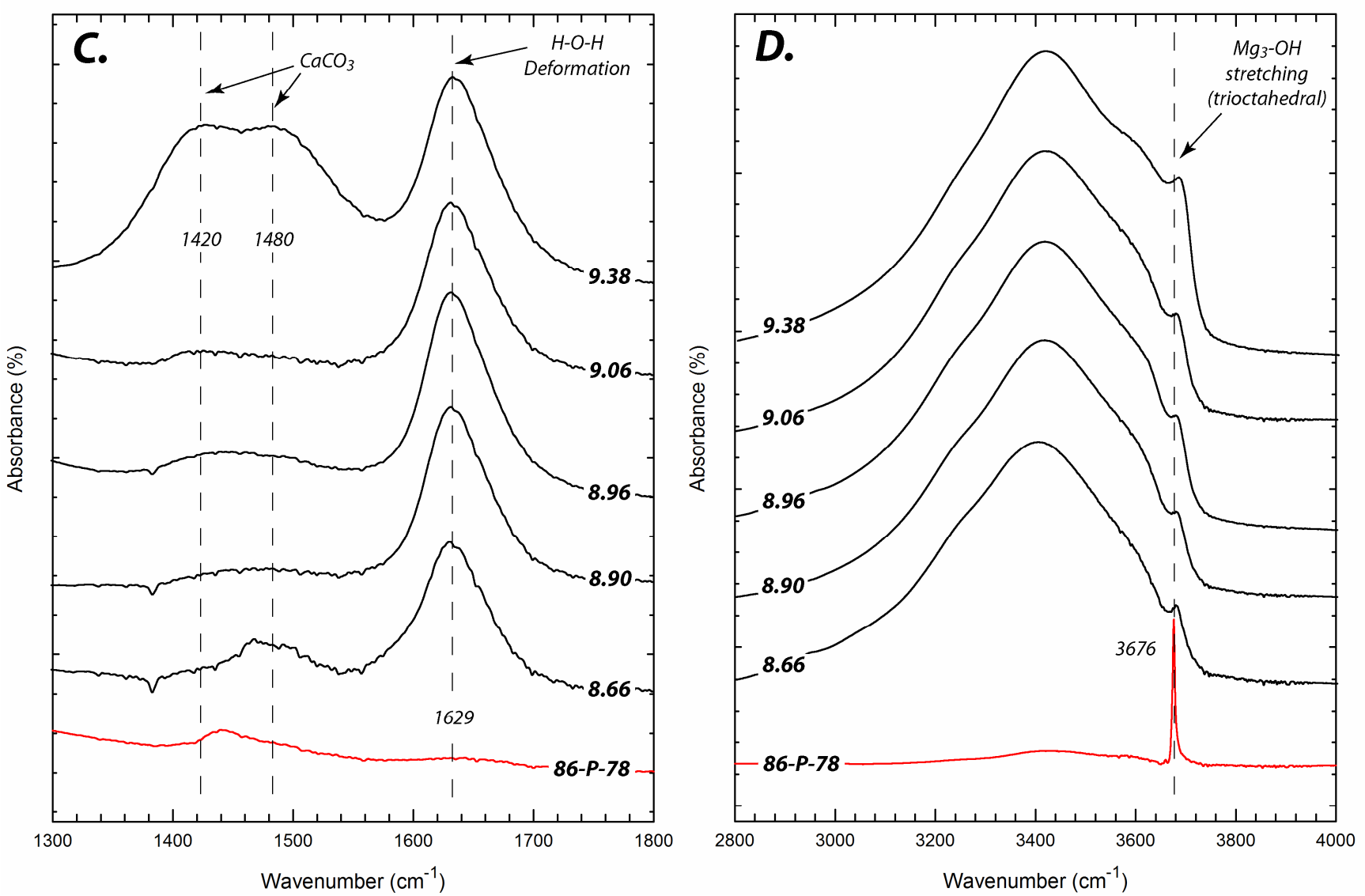
C.
CaCO3
H-O-H
Deformation
1420
1480
9.38
9.06
8.96
8.90
8.66
1629
86-P-78
Absorbance (%)
1300
1400
1500
1600
1700
1800
Wavenumber (cm-1)
D.
Mg3-OH
stretching
(trioctahedral)
9.38
9.06
8.96
8.90
8.66
3676
86-P-78
Absorbance (%)
2800
3000
3200
3400
3600
3800
4000
Wavenumber (cm-1)

Figure 7.

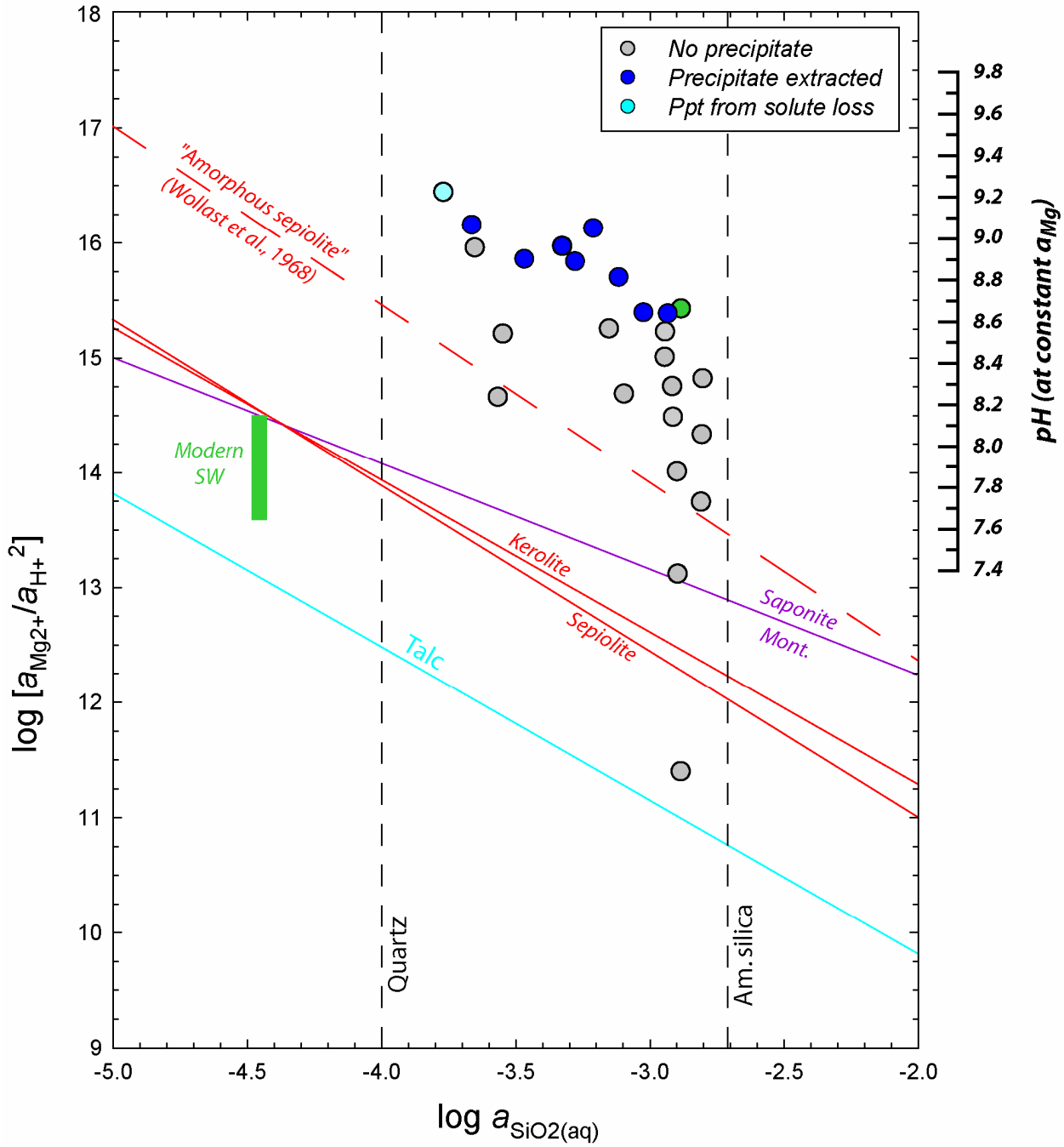
No precipitate
Precipitate extracted
Ppt from solute loss
"Amorphous sepiolite"
(Wollast et al., 1968)
Modern
SW
Kerolite
Sepiolite
Saponite
Mont.
Talc
Quartz
Am. silica
log [a_{Mg2+}/a_{H+}^2]
log $a_{SiO2(aq)}$
pH (at constant a_{Mg})
18
17
16
15
14
13
12
11
10
9
-5.0
-4.5
-4.0
-3.5
-3.0
-2.5
-2.0
9.8
9.6
9.4
9.2
9.0
8.8
8.6
8.4
8.2
8.0
7.8
7.6
7.4

Figure 8.

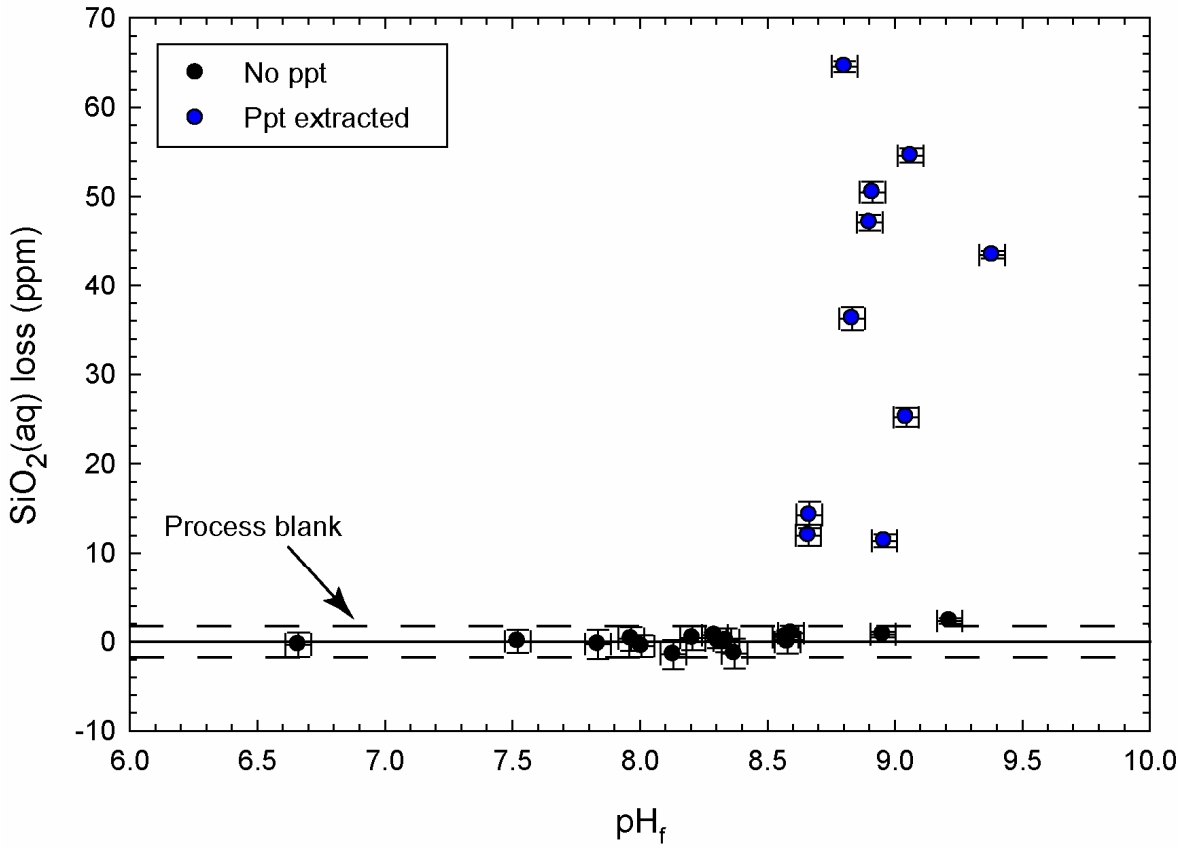
No ppt
Ppt extracted
Process blank
SiO_2(aq) loss (ppm)
pH_f
70
60
50
40
30
20
10
0
-10
6.0
6.5
7.0
7.5
8.0
8.5
9.0
9.5
10.0

Figure 9.

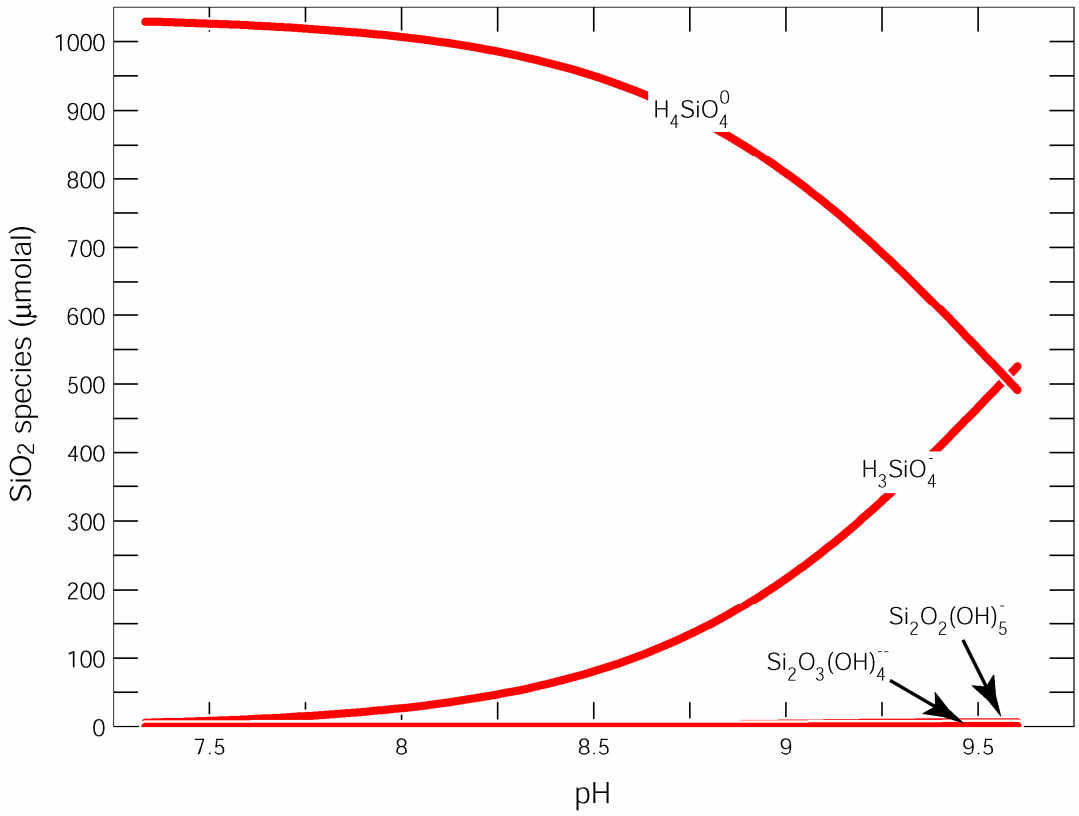
1000
900
800
700
600
500
400
300
200
100
0
SiO2 species (µmolal)
H4SiO40
H3SiO4-
Si2O2(OH)5-
Si2O3(OH)4--
7.5
8
8.5
9
9.5
pH

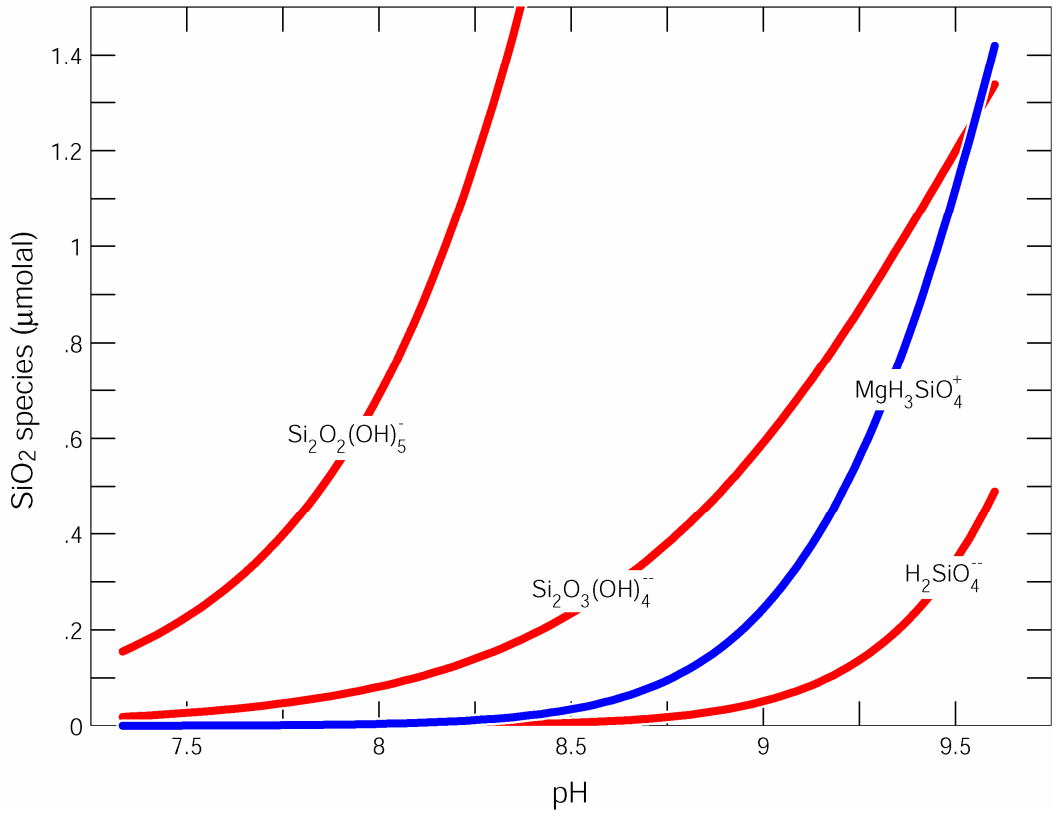
1.4
1.2
1
.8
.6
.4
.2
0
SiO2 species (µmolal)
Si2O2(OH)5-
Si2O3(OH)4--
MgH3SiO4+
H2SiO4--
7.5
8
8.5
9
9.5
pH

Supplemental Data File (Tosca et al., Sedimentary talc in Neoproterozoic carbonate successions)

Mineralogical and geochemical analyses

Mineralogical analyses were performed on samples that were first cut on all sides to expose fresh surfaces. Samples were processed with a jaw crusher and then by hand in an agate mortar and pestle. To aid carbonate dissolution, some samples were pre-ground in an agate swing mill for <1-2 minutes at 200 rpm. Powders were again hand ground in an agate mortar and pestle, and dissolution was performed by step-wise addition of 0.3 mol/kg acetic acid. Solutions were monitored for effervescence to ensure that pH values did not drop below 4, minimizing Mg-silicate structural modification or dissolution (Moore and Reynolds Jr., 1997; Yebra-Rodriguez et al., 2003). Samples were repeatedly rinsed and re-suspended in de-ionized water with sodium phosphate as a dispersal agent and sonicated. The <2μm fraction was then separated by gravity settling and transferred to a clean glass slide in preparation for XRD using a filter-peel technique (Moore and Reynolds Jr., 1997). Samples were analyzed as air-dried oriented aggregates and again after ethylene glycol solvation by exposure to ethylene glycol vapor overnight at 60^{o}C.

X-ray diffraction of clay separates and bulk samples was performed with a Bruker D-8 Advance powder diffractometer with a Cu Kα radiation at 40 kV and 30mA and also with a Siemens D5000 diffractometer at 30 kV and 20mA. Divergent slit sizes of 0.2 mm and receiving and anti-scatter slit sizes of 0.6 and 1.0 mm, respectively, were used. For oriented aggregates, samples were analyzed at intervals of 0.03 degrees with 4-8 seconds counting per step. Randomly oriented samples were analyzed from 3-65 degrees at 4 seconds per 0.02^{o} step, with <2μm size fractions randomly oriented and analyzed from 50-65 degrees at 30 seconds per step to resolve weak 060 peaks that constrain octahedral occupancy. Electron microprobe analysis was performed on polished and carbon-coated thin sections with a Cameca SX-100 electron microprobe equipped with 5 wavelength dispersive spectrometers, capable of analyzing elements from B to U.

Experimental procedure

The source of aqueous silica used in the experiments was a 99.9% reagent-grade anhydrous tetraethoxysilane (or TEOS) solution, which, upon contact with water, rapidly

hydrolyzes, producing SiO_2(aq) and a small amount of residual ethanol. Although the hydrolysis of organo-silica complexes is rapid, there is a well-documented lag period during which the initially introduced SiO_2(aq) de-polymerizes and reaches equilibrium with the surrounding solution in mostly monomeric (i.e., H_4SiO_4) form (Dietzel, 2000; Iler, 1979). With this in mind, all SiO_2(aq) introduced in the experiment was given enough time to de-polymerize and equilibrate in the solution before Mg was introduced as $MgCl_2$(aq).

Aqueous samples (1 mL) were periodically extracted from the experiments and immediately filtered with 0.2 μm syringe-driven nylon filters, acidified and stored for analysis. Solution samples were analyzed for major element chemistry using a Varian Vista Pro simultaneous ICP-AES. Calibration was performed with eight standard solutions bracketing expected sample concentrations. In addition, two external quality control standards (matrix matched) were periodically analyzed with samples to determine external precision (0.44% relative standard deviation for Mg and Si, and 0.69% for Ca) and accuracy (0.57-1.03%).

At experiment termination, remaining solution was filtered through a 0.2 μm nylon filter membrane to extract any solid precipitate that formed over the course of the incubation period. Solid precipitates were dried overnight at 50^{o}C and prepared as oriented aggregates and randomly oriented samples for XRD analysis. Solid samples were also analyzed by FT-IR using a Bruker IFS 66v infrared spectrometer. IR measurements were collected on KBr pellets with a sample:KBr ratio of 1:300. Measurements were collected from 350-5000 cm^{-1} at 1 cm^{-1} resolution using a DTGS detector with a KBr window and beamsplitter. Selected samples were prepared for TEM analysis by dispersion in ethanol and deposition on Cu grids.

In addition to experiments run at 25^{o}C, selected solid precipitates were loaded in Teflon vessels with deionized water at a solid:water ratio of 1:75. These experiments were run in hydrothermal bombs at 180 ±1^{o}C for 2-4 weeks to simulate the effects of burial and heating on seawater precipitates over the course of burial diagenesis. Higher temperature experiments were run with precipitate and deionized water (at a solid:water ratio of 1:75) sealed in Au tubes and loaded into a cold-seal hydrothermal apparatus. Experiments were run at 3-4 days at 400^{o}C and 1 kbar hydrostatic pressure.

Thermodynamic speciation calculations

Thermodynamic speciation calculations for SiO_2(aq)-bearing seawater were performed with Geochemists Workbench using a Pitzer-based method for ion activity coefficient calculation based on models developed by Harvie et al. (1984) and Marion and Farren (1999) for major seawater components. For silica speciation in solution, we included H_4SiO_4 dissociation constants from Hershey and Millero (1986) and Pitzer coefficients for SiO_2 species calculated by Felmy et al. (2001). We also included aqueous silica complexes from Felmy et al. (2001) and Santschi and Schindler (1974). Speciation calculations discussed in the text were conducted as follows: initial low-SO_4 (2.8 mmol/kg) Al- and Fe-free seawater compositions were equilibrated with 60 mg/kg SiO2(aq) and a CO_2-containing atmosphere at a pCO_2 to yield an initial pH of 7.25 (log fCO_2 = -1.0). CO_2 fugacity was then decreased while maintaining equilibrium with seawater by pH adjustment until the final seawater pH reached ~9.7 at a log fCO_2 = -4.0.

Details of clay mineral identification

Saponite was identified by a strong basal 001 reflection in air dried oriented aggregates which shifted to 16.1 Å after ethylene glycol treatment. XRD analyses of randomly oriented <2μm powders revealed a 060 peak at 1.529Å, corresponding to trioctahedral occupancy. The saponite was found only in samples from the Hunnberg Formation. One sample dominated entirely by finely laminated dolomicrite and abundant molar tooth structures yielded almost pure saponite (with a small amount of R1 illite(0.5)/smectite) after decarbonation.

Corrensite, a mixed layered regularly ordered chlorite(0.5)/smectite was identified in one sample from the Svanbergfjellet Formation (86-G-3). An intense superstructure 001* reflection in both the air dried and ethylene glycol-solvated states, along with a rational series of 00*l* reflections upon ethylene glycol-solvation, were sufficient to unambiguously identify corrensite in this sample. The corrensite is of the trioctahedral low-charge variety, indicating that the chlorite component is mixed with trioctahedral saponite.

Figure 4B in the manuscript shows an XRD pattern of the <2μm decarbonated residue from sample K2016 (Hunnberg Fm). Talc can be clearly identified from the reflection at 9.37Å. However, the broad peak centered at ~6 degrees 2Θ contains two reflections: 14.7 Å and 13.3 Å in the air-dried state, and at 16.5 Å and 14.9 Å in the EG-solvated state. From high angle XRD scans of random powders, an 060 peak is present at 1.528 Å, which, combined with reflections at 14.7 and 16.5 Å in air-dried and EG-solvated, respectively, can be identified as saponite. The 00*l*

reflections of the additional phase are all well-matched by R1 chlorite(0.75)/smectite. Calculated X-ray diffraction patterns of this phase (using the program NEWMOD; (Reynolds Jr. and Reynolds, 1996)) correspond precisely with observed reflections throughout the 00*l* series. Such a mixed-layer phase is relatively uncommon in natural samples; corrensite is by far the most common chlorite/smectite species, but other forms of chlorite/smectite mixed layering have been reported in association with carbonate and/or evaporite deposits (e.g., (Hillier, 1993)).

References

Dietzel, M., 2000, Dissolution of silicates and the stability of polysilicic acid: Geochimica et Cosmochimica Acta, v. 64, p. 3275-3281.

Felmy, A.R., Cho, H., Rustad, J.R., and Mason, M.J., 2001, An aqueous thermodynamic model for polymerized silica species to high ionic strength: Journal of Solution Chemistry, v. 30, p. 509-525.

Harvie, C.E., Moller, N., and Weare, J.H., 1984, The prediction of mineral solubilities in natural waters: The Na-K-Mg-Ca-H-Cl-SO_4-OH-HCO_3-CO_3-CO_2-H_2O system to high ionic strengths at 25^{o}C: Geochimica et Cosmochimica Acta, v. 48, p. 723-751.

Hershey, J.P., and Millero, F.J., 1986, The dependence of the acidity constants of silicic acid on NaCl concentrations using Pitzer equations: Marine Chemistry, v. 18, p. 101-105.

Hillier, S., 1993, Origin, Diagenesis, and Mineralogy of Chlorite Minerals in Devonian Lacustrine Mudrocks, Orcadian Basin, Scotland: Clays and Clay Minerals, v. 41, p. 240-259.

Iler, R.K., 1979, The Chemistry of Silica: Solubility, Polymerization, Colloid and Surface Properties, and Biochemistry: New York, Wiley, 866 p.

Marion, G.M., and Farren, R.E., 1999, Mineral solubilities in the Na-K-Mg-Ca-Cl-SO_4-H_2O system: A re-evaluation of the sulfate chemistry in the Spencer-Moller-Weare model: Geochimica et Cosmochimica Acta, v. 63, p. 1305-1318.

Moore, D.M., and Reynolds Jr., R.C., 1997, X-ray diffraction and the identification and analysis of clay minerals: New York, Oxford University Press, 378 p.

Reynolds Jr., R.C., and Reynolds, I., R.C., 1996, NEWMOD for Windows. The calculation of one dimensional X-ray diffraction patterns of mixed-layered clay minerals: Hanover, NH.

Santschi, P.H., and Schindler, P., 1974, Complex-Formation in Ternary-Systems Ca(II)-H4SiO4-H2O and Mg(II)-H4SIO4-H2O: Journal of the Chemical Society-Dalton Transactions, p. 181-184.

Yebra-Rodriguez, A., Martin-Ramos, J.D., del Rey, F., Viseras, C., and Lopez-Galindo, A., 2003, Effect of acid treatment on the structure of sepiolite: Clay Minerals, v. 38, p. 353-360.

Figure 1. Comparison of oriented <2mm fraction (EG-solvated) of sample K2016 from the Hunnberg Formation, Nordaustlandet, Svalbard (A) with (B) a simulated one dimensional X-ray diffraction pattern (calculated by NEWMOD) for a physical mixture of: 67% talc, 27% tri-octahedral smectite (saponite), and 7% R0 tri-tri chlorite 0.7/tri-smectite.

Figure 2. Transmission electron micrograph of poorly crystalline Mg-silicate precipitated at a pH of 8.901 (with selected area electron diffraction pattern shown in inset). Photomicrographs of experimental precipitates show a crinkly morphology at the nanometer scale, and in some regions, the development of hexagonally-shaped particles. Some regions of the precipitate exhibit observable patterns in selected area electron diffraction implying crystalline order at the nanometer scale. The smearing of diffracted spots into weak circular patterns is consistent with low stacking order in the *z* direction.

Table 1. Experimental conditions

Expt ID	*pH_f*	*$[SiO_2]_i$ (ppm)*	*$[Mg]_i$ (ppm)*	*Composition*	*Precipitate*
MgSi_1	6.661	69.70	1182	SW (2.8 mmol/kg SO_4)	--
MgSi_2	7.521	68.80	1181	SW (2.8 mmol/kg SO_4)	--
MgSi_3	7.966	69.88	1178	SW (2.8 mmol/kg SO_4)	--
MgSi_4	8.339	69.17	1178	SW (2.8 mmol/kg SO_4)	--
MgSi_5	8.661	69.39	1180	SW (2.8 mmol/kg SO_4)	PCMS
MgSi_6	8.901	69.39	1180	SW (2.8 mmol/kg SO_4)	PCMS
MgSi_7	8.307	45.53	1165	SW (2.8 mmol/kg SO_4)	--
MgSi_8	8.593	42.87	1159	SW (2.8 mmol/kg SO_4)	--
MgSi_9	8.959	43.04	1167	SW (2.8 mmol/kg SO_4)	PCMS
MgSi_10	9.382	43.81	1157	SW (2.8 mmol/kg SO_4)	Corr; pc-Talc
MgSi_11	8.294	16.07	1165	SW (2.8 mmol/kg SO_4)	--
MgSi_12	8.570	17.25	1165	SW (2.8 mmol/kg SO_4)	--
MgSi_13	8.953	15.70	1165	SW (2.8 mmol/kg SO_4)	--
MgSi_14	9.215	15.50	1165	SW (2.8 mmol/kg SO_4)	--
MgSi_15	9.062	69.90	1165	SW (2.8 mmol/kg SO_4)	PCMS
MgSi_16	7.835	84.70	1174	SW (2.8 mmol/kg SO_4)	--
MgSi_17	8.131	85.06	1171	SW (2.8 mmol/kg SO_4)	--
MgSi_18	8.371	85.65	1168	SW (2.8 mmol/kg SO_4)	--
MgSi_19	8.665	85.14	1195	SW (2.8 mmol/kg SO_4)	PCMS
MgSi_20	8.833	85.14	1200	SW (2.8 mmol/kg SO_4)	PCMS
MgSi_21	8.912	85.14	1175	SW (2.8 mmol/kg SO_4)	PCMS
MgSi_22	8.207	68.92	1164	SW (28 mmol/kg SO_4)	--
MgSi_23	8.579	67.75	1165	SW (28 mmol/kg SO_4)	--
MgSi_24	9.044	68.34	1164	SW (28 mmol/kg SO_4)	PCMS
MgSi_25	8.007	62.94	12900	SW (2.8 mmol/kg SO_4)	--
MgSi_26	8.803	64.88	12900	SW (2.8 mmol/kg SO_4)	PCMS

PCMS: *Poorly crystalline Mg-silicate*
pc-Talc: *Poorly crystalline talc*
Corr: *Corrensite (trioctahedral)*

Figure 1.

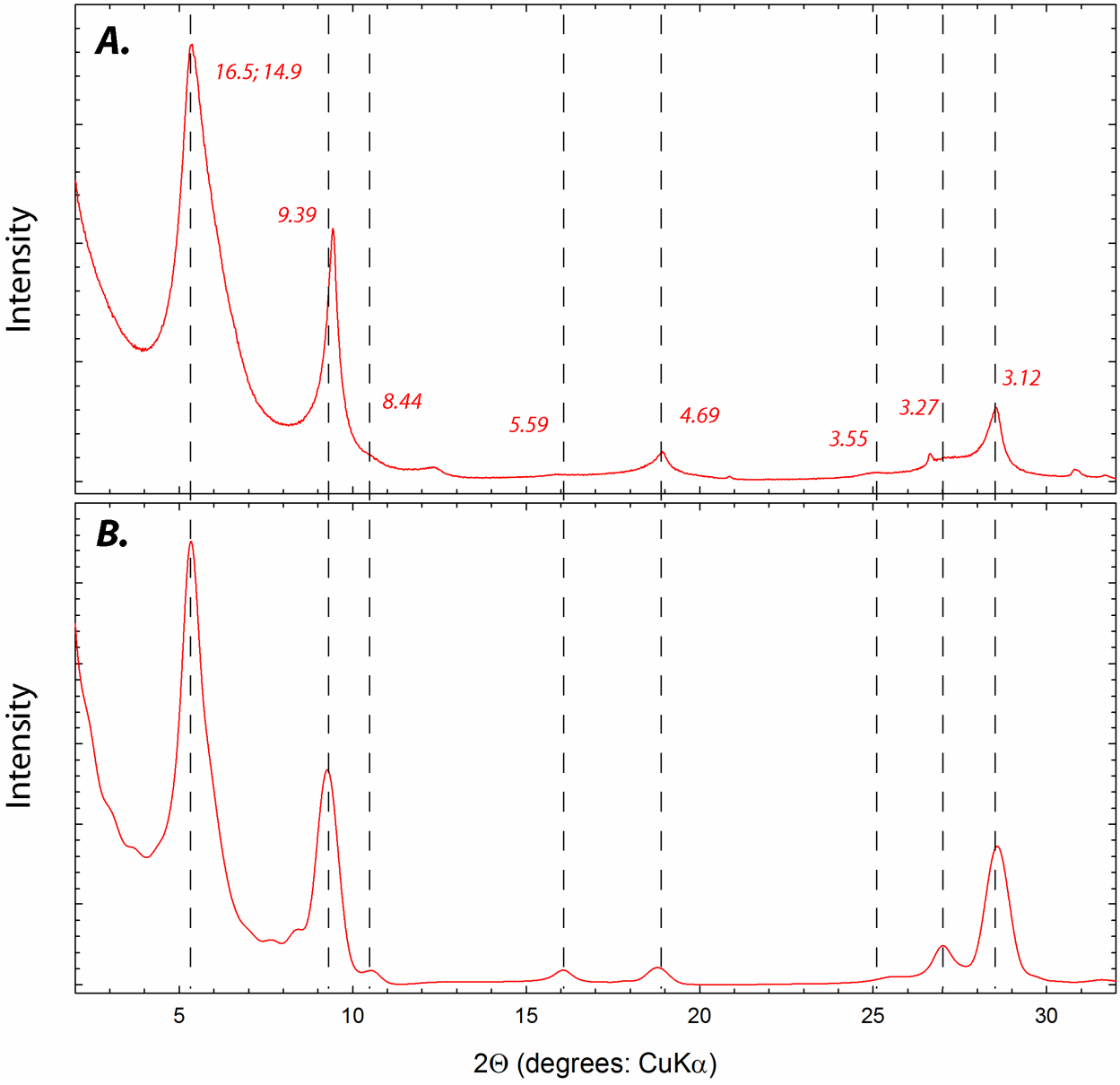
A.
16.5; 14.9
9.39
8.44
5.59
4.69
3.55
3.27
3.12
Intensity
B.
Intensity
5
10
15
20
25
30
2Θ (degrees: CuKα)

Figure 2.